FLUXNET-CH4: A global, multi-ecosystem dataset and analysis of methane seasonality from freshwater wetlands

Kyle B. Delwiche[1], Sara Helen Knox[2], Avni Malhotra[1], Etienne Fluet-Chouinard[1], Gavin McNicol[1], Sarah Feron[1,3], Zutao Ouyang[1], Dario Papale[4,5], Carlo Trotta[5], Eleonora Canfora[5], You-Wei Cheah[6], Danielle Christianson[6], Ma. Carmelita R. Alberto[7], Pavel Alekseychik[8], Mika Aurela[9], Dennis Baldocchi[10], Sheel Bansal[11], David P. Billesbach[12], Gil Bohrer[13], Rosvel Bracho[14], Nina Buchmann[15], David I. Campbell[16], Gerardo Celis[17], Jiquan Chen[18], Weinan Chen[19], Housen Chu[20], Higo J Dalmagro[21], Sigrid Dengel[6], Ankur R Desai[22], Matteo Detto[23], Han Dolman[24], Elke Eichelmann[25], Eugenie Euskirchen[26], Daniela Famulari[27], Kathrin Fuchs[28], Mathias Goeckede[29], Sébastien Gogo[30], Mangaliso J. Gondwe[31], Jordan P Goodrich[16], Pia Gottschalk[32], Scott L. Graham[33], Martin Heimann[29], Manuel Helbig[34,35], Carole Helfter[36], Kyle S. Hemes[1,37], Takashi Hirano[38], David Hollinger[39], Lukas Hörtnagl[15], Hiroki Iwata[40], Adrien Jacotot[30], Gerald Jurasinski[41], Minseok Kang[42], Kuno Kasak[43], John King[44], Janina Klatt[45], Franziska Koebsch[41], Ken W Krauss[46], Derrick Y.F. Lai[47], Annalea Lohila[9,48], Ivan Mammarella[48], Giovanni Manca[49], Luca Belelli Marchesini[50], Jaclyn Hatala Matthes[51], Trofim Maximon[52], Lutz Merbold[53], Bhaskar Mitra[54], Timothy H. Morin[55], Eiko Nemitz[36], Mats B. Nilsson[56], Shuli Niu[19], Walter C Oechel[57], Patricia Y. Oikawa[58], Keisuke Ono[59], Matthias Peichl[56], Olli Peltola[9], Michele L. Reba[60], Andrew D. Richardson[61,62], William Riley[6], Benjamin R. K. Runkle[63], Youngryel Ryu[64], Torsten Sachs[32], Ayaka Sakabe[65], Camilo Rey Sanchez[10], Edward A Schuur[66], Karina VR Schäfer[67], Oliver Sonnentag[68], Jed P. Sparks[69], Ellen Stuart-Haëntjens[70], Cove Sturtevant[71], Ryan C. Sullivan[72], Daphne J. Szutu[10], Jonathan E Thom[73], Margaret S. Torn[6], Eeva-Stiina Tuittila[74], Jessica Turner[75], Masahito Ueyama[76], Alex C. Valach[10], Rodrigo Vargas[77], Andrej Varlagin[78], Alma Vazquez-Lule[77], Joseph G. Verfaillie[10], Timo Vesala[48,79], George L Vourlitis[7809], Eric J. Ward[46], Christian Wille[32], Georg Wohlfahrt[81], Guan Xhuan Wong[821], Zhen Zhang[823], Donatella Zona[57, 834], Lisamarie Windham-Myers[845], Benjamin Poulter[856], Robert B. Jackson[1, 37, 867]

[1] Department of Earth System Science, Stanford University, Stanford, California
[2] Department of Geography, The University of British Columbia, Vancouver, British Columbia, Canada
[3] Department of Physics, University of Santiago de Chile, Santiago, Chile
[4] Dipartimento per la Innovazione nei Sistemi Biologici, Agroalimentari e Forestali, Università degli Studi della Tuscia, Largo dell'Universita, Viterbo, Italy e Forestali, Universita
[5] euroMediterranean Center on Climate Change CMCC, Lecce, Italy
[6] Earth and Environmental Sciences Area, Lawrence Berkeley National Lab, Berkeley, California
[7] International Rice Research Institute, Los Banos, Laguna, Philippines
[8] Natural Resources Institute Finland (LUKE), Helsinki, Finland
[9] Finnish Meteorological Institute, PO Box 501, 00101 Helsinki, Finland
[10] Department of Environmental Science, Policy and Management, University of California, Berkeley, CA, USA
[11] U.S. Geological Survey, Northern Prairie Wildlife Research Center, 8711 37th St Southeast, Jamestown, ND 58401 USA
[12] University of Nebraska-Lincoln, Department of Biological Systems Engineering, Lincoln, NE 68583, USA
[13] Department of Civil, Environmental & Geodetic Engineering, Ohio State University
[14] School of Forest Resources and Conservation, University of Florida, Gainesville FL, 32611

[15] Department of Environmental Systems Science, Institute of Agricultural Sciences, ETH Zurich, 8092 Zurich, Switzerland
[16] School of Science, University of Waikato, Hamilton, New Zealand
[17] Agronomy Department, University of Florida, Gainesville FL, 32601
[18] Department of Geography, Environment, and Spatial Sciences, Michigan State University, East Lansing, MI 48823, USA
[19] Institute of Geographic Sciences and Natural Resources Research, Chinese Academy of Sciences, Beijing 100101, PR China.
[20] Climate and Ecosystem Sciences Division, Lawrence Berkeley National Lab, Berkeley, CA 94702, USA
[21] Universidade de Cuiaba, Cuiaba, Mato Grosso, Brazil
[22] Dept of Atmospheric and Oceanic Sciences, University of Wisconsin-Madison, Madison, WI 53706 USA
[23] Department of Ecology and Evolutionary Biology, Princeton University, Princeton NJ, USA
[24] Department of Earth Sciences, Vrije Universiteit, Amsterdam, Netherlands
[25] School of Biology and Environmental Science, University College Dublin, Ireland
[26] University of Alaska Fairbanks, Institute of Arctic Biology, Fairbanks, AK, USA
[27] C NR - institute for Mediterranean Agricultural and Forest Systems, Piazzale Enrico Fermi, 1 Portici (Napoli) Italy
[28] Institute of Meteorology and Climate Research - Atmospheric Environmental Research, Karlsruhe Institute of Technology (KIT Campus Alpin), 82467 Garmisch-Partenkirchen, Germany
[29] Max Planck Institute for Biogeochemistry, Jena, Germany
[30] ISTO, Université d'Orléans, CNRS, BRGM, UMR 7327, 45071, Orléans, France
[31] Okavango Research Institute, University of Botswana, Maun, Botswana.
[32] GFZ German Research Centre for Geosciences, Telegrafenberg, 14473 Potsdam, Germany
[33] Manaaki Whenua - Landcare Research, Lincoln, NZ
[34] Université de Montréal, Département de géographie, Université de Montréal, Montréal, QC H2V 0B3,
[35] Canada & Dalhousie University, Department of Physics and Atmospheric Science, Halifax, NS B2Y 1P3, Canada
[36] UK Centre for Ecology and Hydrology, Edinburgh, UK
[37] Woods Institute for the Environment, Stanford University, Stanford, California
[38] Research Faculty of Agriculture, Hokkaido University, Sapporo, Japan
[39] Northern Research Station, USDA Forest Service, Durham, NH 03824, USA
[40] Department of Environmental Science, Faculty of Science, Shinshu University
[41] University of Rostock, Rostock, Germany
[42] National Center for Agro Meteorology, Seoul, South Korea
[43] Department of Geography, University of Tartu, Vanemuise st 46, Tartu, 51410, Estonia
[44] Department of Forestry and Environmental Resources, North Carolina State University, Raleigh, NC, USA
[45] Vegetation Ecology, Institute of Ecology and Landscape, Department Landscape Architecture, Weihenstephan-Triesdorf University of Applied Sciences, Am Hofgarten 1, 85354 Freising, Germany
[46] U.S. Geological Survey, Wetland and Aquatic Research Center, Lafayette LA
[47] Department of Geography and Resource Management, The Chinese University of Hong Kong, Shatin, New Territories, Hong Kong SAR, China
[48] Institute for Atmospheric and Earth System Research/Physics, Faculty of Science, University of Helsinki, Helsinki, Finland
[49] European Commission, Joint Research Centre (JRC), Ispra, Italy.
[50] Dept. of Sustainable Agro-Ecosystems and Bioresources, Research and Innovation Centre, Fondazione Edmund Mach, San Michele all'Adige , Italy
[51] Department of Biological Sciences, Wellesley College, Wellesley, MA 02481, USA
[52] Institute for Biological Problems of the Cryolithozone, RAS, Yakutsk, REp. Yakutia.
[53] Mazingira Centre, International Livestock Research Institute (ILRI), Old Naivasha Road, PO Box 30709, 00100 Nairobi, Kenya
[54] Northern Arizona University, School of Informatics, Computing and Cyber Systems
[55] Environmental Resources Engineering, SUNY College of Environmental Science and Forestry
[56] Dept. of Forest Ecology and Management, Swedish University of Agricultural Sciences, 901 83 Umeå, Sweden
[57] Dept. Biology, San Diego State University, San Diego, CA 92182, USA
[58] Department of Earth and Environmental Sciences, Cal State East Bay, Hayward CA 94542 USA
[59] National Agriculture and Food Research Organization, Tsukuba, Japan
[60] USDA-ARS Delta Water Management Research Unit, Jonesboro, Arkansas 72401, United States

[61] School of Informatics, Computing & Cyber Systems, Northern Arizona University, Flagstaff, AZ 86011, USA
[62] Center for Ecosystem Science and Society, Northern Arizona University, Flagstaff, AZ 86011, USA
[63] Department of Biological & Agricultural Engineering, University of Arkansas, Fayetteville, Arkansas 72701, United States
[64] Department of Landscape Architecture and Rural Systems Engineering, Seoul National University, South Korea
[65] Hakubi center, Kyoto University, Kyoto, Japan
[66] Department of Biological Sciences, Northern Arizona University, Flagstaff, AZ, USA
[67] Dept of Earth and Environmental Science, Rutgers University Newark, NJ
[68] Université de Montréal, Département de géographie, Université de Montréal, Montréal, QC H2V 0B3, Canada
[69] Department of Ecology and Evolution, Cornell
[70] U.S. Geological Survey, California Water Science Center, 6000 J Street, Placer Hall, Sacramento, CA, 95819
[71] National Ecological Observatory Network, Battelle, 1685 38th St Ste 100, Boulder, Colorado, 80301, USA
[72] Environmental Science Division, Argonne National Laboratory, Lemont, IL, USA
[73] Space Sciences and Engineering Center, University of Wisconsin-Madison, Madison, WI 53706 USA
[74] School of Forest Sciences, University of Eastern Finland, Joesnuu, Finland
[75] Freshwater and Marine Science, University of Wisconsin-Madison
[76] Graduate School of Life and Environmental Sciences, Osaka Prefecture University
[77] Department of Plant and Soil Sciences, University of Delaware, Newark, DE, USA
[78] A.N. Severtsov Institute of Ecology and Evolution, Russian Academy of Sciences
[79] Yugra State University, 628012, Khanty-Mansiysk, Russia
[~~79~~80] California State University San Marcos, San Marcos, CA, USA
[81~~0~~] University of Innsbruck, Department of Ecology, Sternwartestr. 15, 6020 Innsbruck, AUSTRIA
[82~~1~~] Sarawak Tropical Peat Research Institute, Sarawak, Malaysia
[83~~2~~] Department of Geographical Sciences, University of Maryland, College Park, MD 20740, USA
[84~~3~~] Department of Animal and Plant Sciences, University of Sheffield, Western Bank, Sheffield, S10 2TN, United Kingdom
[85~~4~~] U.S. Geological Survey,Water Mission Area, 345 Middlefield Road, Menlo Park, CA, 94025
[86~~5~~] Biospheric Sciences Laboratory, NASA Goddard Space Flight Center, Greenbelt, Maryland
[87~~6~~] Precourt Institute for Energy, Stanford University, Stanford, California

Correspondence to: Kyle B. Delwiche (delwiche@stanford.edu)

Abstract. Methane (CH_4) emissions from natural landscapes constitute roughly half of global CH_4 contributions to the atmosphere, yet large uncertainties remain in the absolute magnitude and the seasonality of emission quantities and drivers. Eddy covariance (EC) measurements of CH_4 flux are ideal for constraining ecosystem-scale CH_4 emissions due to quasi-continuous and high temporal resolution of CH_4 flux measurements, coincident carbon dioxide, water, and energy flux measurements, lack of ecosystem disturbance, and increased availability of datasets over the last decade. Here, we 1) describe the newly published dataset, FLUXNET-CH4 Version 1.0, the first, open source global dataset of CH_4 EC measurements (available at https://fluxnet.org/data/fluxnet-ch4-community-product/). FLUXNET-CH4 includes half-hourly and daily gap-filled and non gap-filled aggregated CH_4 fluxes and meteorological data from 79 sites globally: 42 freshwater wetlands, 6 brackish and saline wetlands, 7 formerly drained ecosystems, 7 rice paddy sites, 2 lakes, and 15 uplands. Then, we 2) evaluate FLUXNET-CH4 representativeness for freshwater wetland coverage globally, because the majority of sites in FLUXNET-CH4 Version 1.0 are freshwater wetlands which are a substantial source of total atmospheric CH_4 emissions; and 3) provide the first global estimates of the seasonal variability and seasonality predictors of freshwater wetland CH_4 fluxes. Our representativeness analysis suggests that the freshwater wetland sites in the dataset cover global wetland bioclimatic attributes (encompassing energy, moisture, and vegetation-related parameters) in arctic, boreal, and temperate regions, but only sparsely cover humid tropical regions. Seasonality metrics of wetland CH_4 emissions vary considerably across latitudinal bands. In freshwater wetlands (except those between 20° S to 20° N) the spring onset of elevated CH_4 emissions starts three

days earlier, and the CH_4 emission season lasts 4 days longer, for each degree C increase in mean annual air temperature. On average, the spring onset of increasing CH_4 emissions lags soil warming by one month, with very few sites experiencing increased CH_4 emissions prior to the onset of soil warming. In contrast, roughly half of these sites experience the spring onset of rising CH_4 emissions prior to the spring increase in gross primary productivity (GPP). The timing of peak summer CH_4 emissions does not correlate with the timing for either peak summer temperature or peak GPP. Our results provide seasonality parameters for CH_4 modeling, and highlight seasonality metrics that cannot be predicted by temperature or GPP (i.e., seasonality of CH_4 peak). FLUXNET-CH4 is a powerful new resource for diagnosing and understanding the role of terrestrial ecosystems and climate drivers in the global CH_4 cycle; and future additions of sites in tropical ecosystems and site-years of data collection will provide added value to this database. All seasonality parameters are available at https://doi.org/10.5281/zenodo.4672601. Additionally, raw FLUXNET-CH4 data used to extract seasonality parameters can be downloaded from https://fluxnet.org/data/fluxnet-ch4-community-product/, and a complete list of the 79 individual site data DOIs is provided in Table 2 in the Data Availability section of this document.

1 Introduction

Methane (CH_4) has a global warming potential that is 28 times larger than carbon dioxide (CO_2) on a 100-year time scale (Myhre et al., 2013), and its atmospheric concentration has increased by >1000 ppb since 1800 (Etheridge et al., 1998). While atmospheric CH_4 concentrations are substantially lower than those of CO_2, CH_4 has contributed 20-25% as much radiative forcing as CO_2 since 1750 (Etminan et al., 2016). Despite its importance to global climate change, natural CH_4 sources and sinks remain poorly constrained, and with uncertain attribution to the various biogenic and anthropogenic sources (Saunois et al., 2016, 2020). Bottom-up and top-down estimates differ by 154 Tg/yr (745 versus 591 Tg/yr, respectively); much of this difference arises from natural sources (Saunois et al., 2020). Vegetated wetlands and inland water bodies account for most natural CH_4 emissions, as well as the majority of uncertainty in bottom-up emissions estimates (Saunois et al., 2016). Better diagnosis and prediction of terrestrial CH_4 sources to the atmosphere requires high frequency and continuous measurements of CH_4 exchange across a continuum of time (hours to years) and space (meters to kilometers) scales.

Tower-based eddy covariance (EC) measurements provide ecosystem-scale CH_4 fluxes at high temporal resolution across years, are coupled with measurements of key CH_4 drivers such as temperature, water and recent substrate input (inferred from CO_2 flux), and thus help constrain bottom-up CH_4 budgets and improve CH_4 predictions. Although EC towers began measuring CO_2 fluxes in the late 1970s (Desjardins 1974; Anderson et al., 1984), and some towers began measuring CH_4 in the 1990s (Verma et al., 1992), most CH_4 flux EC measurements began within the last decade (2010s). Given that many EC CH_4 sites are relatively new, the flux community has only recently compiled them for global synthesis efforts (e.g., Chang et al., 2021~~in press~~) and is still working to standardize CH_4 flux measurements and establish gap-filling protocols (Nemitz et al., 2018; Knox et al., 2019). Furthermore, the growth of EC networks for CH_4 fluxes has sometimes taken place in a relatively *ad hoc* fashion, often at sites that were already measuring CO_2 fluxes or where higher CH_4 fluxes were expected, potentially introducing bias. The representativeness and spatial distribution of CO_2 flux tower networks have been assessed to evaluate its ability to upscale fluxes regionally (Hargrove et al., 2003; Hoffman et al., 2013; Papale et al., 2015; Villarreal et al., 2018, 2019) and globally (Jung et al., 2009; 2020). However, a relatively sparse coverage of CH_4 flux towers prompts the question of how well the current observation network provides a sufficient sampling of global or ecosystem-specific bioclimatic conditions.

Broad-scale wetland CH_4 seasonality estimates, such as when fluxes increase, peak, and decrease and the predictors of seasonality, remain relatively unconstrained across wetlands globally. These key seasonality metrics vary considerably across high-emitting systems such as wetlands and other aquatic systems (Desjardins, 1974; Dise, 1992; Melloh and Crill 1996; Wik et al., 2013; Zona et al., 2016; Treat et al., 2018). Few continuous CH_4 flux datasets across representative site-years make it difficult to establish trends in seasonal dynamics, though monthly or annually aggregated estimates of CH_4 fluxes from different seasons do exist for high latitudes (Zona et al., 2016; Treat et al., 2018). Seasonal variability in freshwater wetland CH_4 fluxes is expected to be driven by changes in air and soil temperature, soil moisture (including water table dynamics), and recent carbon substrate availability, which influence the rates of CH_4 production and consumption (Lai, 2009; Bridgham et al., 2013; Dean et al., 2018). Temperature has widely been found to strongly affect CH_4 flux (Chu et al., 2014; Yvon-Durocher et al., 2014; Sturtevant et al., 2016), but the relationship is complex (Chang et al., 2020) and varies seasonally (Koebsch et al., 2015; Helbig et al., 2017). CH_4 flux is also driven by inundation depth since anoxic conditions are typically necessary for methanogenesis (Lai, 2009; Bridgham et al., 2013), though CH_4 production under bulk-oxic conditions has been observed (Angle et al., 2017). Substrate availability influences CH_4 production potential and is linked with gross primary productivity (GPP) because recent photosynthate fuels methanogenesis though this relationship can vary by ecosystem type, plant functional type and biome (Megonigal et al., 1999; Chanton et al., 2008; Hatala et al., 2012; Lai et al., 2014; Malhotra and Roulet, 2015; Sturtevant et al., 2016). In process models, the seasonality of CH_4 emissions from wetlands globally is primarily constrained by inundation (Poulter et al., 2017), with secondary within-wetland influences from temperature and availability of carbon (C) substrates (Melton et al., 2013; Castro-Morales et al., 2018). Bottom-up and top-down global CH_4 estimates continue to disagree on total CH_4 flux magnitudes and seasonality, including the timing of annual peak emissions (Spahni et al., 2011; Saunois et al., 2020). Thus, the variability and predictors of wetland CH_4 seasonality globally remain a knowledge gap that high-frequency and long-term EC data can help fill.

Here, we first describe Version 1.0 of the FLUXNET-CH4 dataset (available at https://fluxnet.org/data/fluxnet-ch4-community-product/). Version 1.0 of the dataset expands and formalizes the publication of data scattered among regional flux networks as described previously in Knox et al. (2019). FLUXNET-CH4 includes half-hourly and daily gap-filled and non gap-filled aggregated CH_4 fluxes and meteorological data from 79 sites globally: 42 freshwater wetlands, 6 brackish and saline wetlands, 7 formerly drained ecosystems, 7 rice paddy sites, 2 lakes, and 15 upland ecosystems. FLUXNET-CH4 includes an additional 2 wetland sites (RU-Vrk and SE-St1), but they are not available under the CC BY 4.0 data policy and thus are excluded from this analysis. Since the majority of sites in FLUXNET-CH4 Version 1.0 (hereafter referred to solely as “FLUXNET-CH4”) are freshwater wetlands, which are a substantial source of total atmospheric CH_4 emissions, we use the subset of data from freshwater wetlands to evaluate the representativeness of freshwater wetland coverage in the FLUXNET-CH4 dataset relative to wetlands globally, and provide the first assessment of global variability and predictors of freshwater wetland CH_4 flux seasonality. We quantify a suite of CH_4 seasonality metrics and evaluate temperature and GPP (a proxy for recent substrate input) as predictors of seasonality across four latitudinal bands (northern, temperate, subtropical, and tropical). Due to a lack of high-temporal resolution water table data at all sites, our analyses are unable to evaluate the critical role of water table on CH_4 seasonality. Here we provide parameters for better understanding and modeling seasonal variability in freshwater wetland CH_4 fluxes and generate new hypotheses and data resources for future syntheses.

2. Methods

2.1 FLUXNET-CH4 dataset

2.1.1 History and data description

The FLUXNET-CH4 dataset was initiated by the Global Carbon Project (GCP) in 2017 to better constrain the global CH_4 budget (https://www.globalcarbonproject.org/methanebudget/index.htm). Beginning with a kick off meeting in May 2018 in Washington DC, hosted by Stanford University, we coordinated with the AmeriFlux Management Project, the European Ecosystem Fluxes Database, and the ICOS Ecosystem Thematic Centre (ICOS-ETC) to avoid duplication of efforts, as most sites are part of different regional networks (albeit with different data products). We collected and standardized data for FLUXNET-CH4 with assistance from the regional flux networks, AmeriFlux's "Year of Methane", FLUXNET, the EU's Readiness of ICOS for Necessities of Integrated Global Observations (RINGO) project, and a U.S. Geological Survey Powell Center working group. FLUXNET-CH4 is a community-led project, so while we developed it with assistance from FLUXNET, we do not necessarily use standard FLUXNET data variables, formats, or methods.

FLUXNET-CH4 includes gap-filled half-hourly CH_4 fluxes and meteorological variables. Gaps in meteorological variables (TA - air temperature, SW_IN - incoming shortwave radiation, LW_IN - incoming longwave radiation, VPD - vapor pressure deficient, PA - pressure, P - precipitation, WS - wind speed) were filled with the ERA-Interim (ERA-I) reanalysis product (Vuichard and Papale, 2015). We used the REddyProc package (Wutzler et al., 2018) to filter flux values with low friction velocity (u_*) based on relating nighttime u_*, to fill gaps in CO_2, latent heat, and sensible heat fluxes, and to partition net CO_2 fluxes into gross primary production (GPP) and ecosystem respiration (RECO) using both the daytime (Lasslop et al., 2010) and nighttime (Reichstein et al., 2005) approaches. Data gaps of CH_4 flux were filled using artificial neural network (ANN) methods first described in Knox et al. (2015) and in Knox et al. (2019), and summarized here in Sect. 2.1.2. Gap-filled data for gaps exceeding two months are provided and flagged for quality. Please see Table B1 for variable description and units, as well as quality flag information. For the seasonality analysis in this paper we excluded data from gaps exceeding two months, and we encourage future users of FLUXNET-CH4 to critically evaluate gap-filled values from long data gaps before including them in analyses (Dengel et al., 2013; Kim et al., 2020).

In addition to half-hourly data, the FLUXNET-CH4 Version 1.0 release also contains a full set of daily mean values for all parameters except wind direction and precipitation. Daily precipitation is included as the daily sum of the half-hourly data, and daily average wind direction is not included.

2.1.2 Gap-filling methods and uncertainty estimates

As described in Knox et al. (2015) and in Knox et al. (2019), the ANN routine used to gap-fill the CH_4 data was optimized for generalizability and representativeness. To avoid biasing the ANN toward environmental conditions with typically better data coverage (e.g., summer-time and daytime measurements), the explanatory data were divided into a maximum of 15 clusters using a k-means clustering algorithm. Data used to train, test, and validate the ANN were proportionally sampled from these clusters. For generalizability, the simplest ANN architecture with good performance (<5% gain in model accuracy for additional increases in architecture complexity) was selected for 20 extractions of the training, test, and validation data. Within each extraction, each tested ANN architecture was reinitialized 10 times, and the initialization with the lowest root-mean-square-error was selected to avoid local minima. The median of the 20 predictions was used to fill each gap. A standard set of variables available across all sites was used to gap-fill CH_4 fluxes (Dengel et al., 2013), which included the previously mentioned meteorological variables TA, SW_IN, WS, PA, and sine and cosine functions to represent seasonality. These meteorological variables were selected for their relevance to CH_4 exchange and were gap-filled using the ERA-I reanalysis data. Other variables related to CH_4 flux (e.g., water table depth [WTD] and soil temperature [TS]) were not included as explanatory variables as they were not available across all sites or had large gaps that could not be filled using the ERA-I reanalysis data (Knox et al., 2019). The ANN gap- filling was performed using MATLAB (MathWorks 2018, version 9.4.0).

While the median of the 20 predictions was used to fill each gap, the spread of the predictions was used to provide a measure of uncertainty resulting from the ANN gap-filling procedure. Specifically, the combined annual gap-filling and random uncertainty was calculated from the variance of the cumulative sums of the 20 ANN predictions (Knox et al., 2015; Anderson et al., 2016; Oikawa et al., 2017). The (non-cumulative) variance of the 20 ANN predictions was also used to provide gap-filling uncertainty for each half-hourly gap-filled value. While this output is useful for data-model comparisons, it cannot be used to estimate cumulative annual gap-filling error because gap-filling error is not random, which is why the cumulative sums of the 20 ANN predictions are used to estimate annual gap-filling error.

Random errors in EC fluxes follow a double exponential (Laplace) distribution with the standard deviation varying with flux magnitude (Richardson et al., 2006; Richardson et al., 2012). For half-hourly CH_4 flux measurements, random error was estimated using the residuals of the median ANN predictions, providing a conservative "upper limit" estimate of the random flux uncertainty (Moffat et al., 2007; Richardson et al., 2008). The annual cumulative uncertainty at 95% confidence was estimated by adding the cumulative gap-filling and random measurement uncertainties in quadrature (Richardson and Hollinger, 2007; Anderson et al., 2016). Annual uncertainties in CH_4 flux for individual site-years are provided in Table B2. Throughout this paper, we include uncertainties on individual site years when discussing single years of data. In sites with multiple years of data, we report the standard deviation of the multiple years.

2.1.3 Dataset structure and site metadata

FLUXNET-CH4 contains two comma-separated data files per site at half-hourly and daily resolutions which are available for download at https://fluxnet.org/data/fluxnet-ch4-community-product/, along with a file containing select site metadata. Each site has a unique FLUXNET-CH4 DOI. All data from the 79 sites used in this analysis are available under CC BY 4.0 (https://creativecommons.org/licenses/by/4.0/) copyright license (FLUXNET-CH4 has an additional 2 sites available under the FLUXNET Tier 2 license (https://fluxnet.org/data/data-policy/), though these sites are not included in our analysis).

Metadata (Table B3) include site coordinates, ecosystem classification based on site literature, presence/absence and dominance for specific vegetation types, and DOI link, as well as calculated data such as annual and quarterly CH_4 flux values. FLUXNET-CH4 Version 1.0 sites were classified based on site-specific literature as fen, bog, swamp, marsh, salt marsh, lake, mangrove, rice paddy/field, wet tundra, upland, or drained ecosystems that previously could have been wetlands, seasonally flooded pastures, or agricultural areas. To the extent possible, we followed classification systems of previous wetland CH_4 syntheses (Olefeldt et al., 2013; Turetsky et al., 2014; Treat et al., 2018). Drained systems are former wetlands that have subsequently been drained but may maintain a relatively shallow water table, which can contribute to occasional methane emissions, although we do not have specific water table depth information at all drained sites. Upland ecosystems are further divided into alpine meadows, grasslands, needleleaf forests, mixed forest, crops, tundra, and urban. Freshwater wetland classifications follow hydrological definitions of bog (ombrotrophic), fen (minerotrophic), wet tundra, marshes and swamps, and were designated as per primary literature on the site. For all sites, vegetation was classified for presence or absence of brown mosses (all species from the division Bryophyta except those in the class Sphagnopsida), *Sphagnum* mosses (any species from class Sphagnopsida), ericaceous shrubs, trees (of any height) and aerenchymatous species (mostly Order Poales but includes exceptions). These categories closely follow Treat et al., (2018), except that aerenchymatous species had to be expanded beyond Cyperaceae to incorporate wetlands globally. Presence/absence of vegetation groups was designated based on species lists in primary literature from the site. Out of the vegetation groups present, the dominant (most abundant) group is also reported and is based on information provided by lead site investigators.

In addition to the variable description table (Table B1) and the site metadata (Table B3), we provide several more tables to complement our analysis. Table B4 includes the climatic data used in the representativeness analysis. Table 5 provides seasonality parameters for CH_4 flux, air temperature, soil temperature (from the probe closest to the ground surface), and GPP. For sites with multiple soil temperature probes, the full set of soil temperature parameters are in Table B6. Table B7 contains the soil temperature probe depths. Table B2 contains the annual CH_4 flux and uncertainty. All Appendix B tables are also available at https://doi.org/10.5281/zenodo.4672601.

2.1.4 Annual CH_4 fluxes

Annual CH_4 fluxes were calculated from gap-filled data for site-years with data gaps shorter than two consecutive months, or for sites above 20° N where >2 month data gaps occurred outside of the highest CH_4-emission months of May 1 through October 31. Since we did not sum gap-filled values for >2 month gaps during the winter, annual sums from these years will be an underestimate since winter fluxes can be important (Zona et al., 2016; Treat et al., 2018). Several sites had less than one year of data, and we report gap-filled CH_4 flux annual sums for sites with between six months and one year of data (BW-Gum = 228 days, CH-Oe2 = 200 days, JP-Swl = 210 days, US-EDN = 182 days). While these sums will be an underestimate of annual CH_4 flux since they do not span a full year (and we therefore do not use them in the seasonality analysis), their relative magnitude can still be informative. For example, site JP-SWL is a lake site, and even with less than a year of data the summed CH_4 flux of 66 g C m^{-2} is relatively high (Taoka et al., 2020). In addition to sites with short time series, the annual CH_4 sum for site ID-Pag represents 365 days spanning June 2016 to June 2017.

2.1.5 Subset analysis on freshwater wetland CH_4 flux

In addition to the FLUXNET-CH4-wide description of site class distributions and annual CH_4 fluxes, we also include a subset analysis on freshwater wetlands, given that it is the dominant ecosystem type in our dataset and an important global CH_4 source (Saunois et al., 2016). First, we analyze freshwater wetland representativeness, and subsequently the seasonality of their CH_4 emissions. Freshwater wetlands included in the seasonality and representativeness analysis are indicated in Table B3, column "IN_SEASONALITY_ANALYSIS".

2.2 Wetland representativeness

2.2.1 Principal Component Analysis

To compare the FLUXNET-CH4 site distribution to the global wetland distribution, we evaluated their representativeness in the entire global wetland cover along four bioclimatic gradients. Only freshwater wetland sites were included in this analysis. Coastal sites were excluded because salinity, an important control on CH_4 production, could not be evaluated across the tower network due to a lack of global gridded salinity data (Bartlett et al., 1987; Poffenbarger et al., 2011). The four bioclimatic variables used were: mean annual air temperature (MAT), latent heat flux (LE), enhanced vegetation index (EVI), and simple ratio water index (SRWI; data sources in Table B4). We use EVI because it is a more direct measurement than GPP from global gridded products and is considered a reasonable proxy for GPP (Sims et al., 2006). Together, these environmental variables account for, or are, proxies for key controls of CH_4 production, oxidation at the surface, and transport (Bridgham et al., 2013). We use a principal components analysis (PCA) to visualize the site distribution across the four environmental drivers at once. For this analysis, we consider the annual average bioclimatic conditions over 2003-2015. In the PCA output, we evaluate the coverage of the 42 freshwater sites over 0.25° grid cells containing >5% wetland mean cover in Wetland Area and Dynamics for Methane Modeling (WAD2M; Zhang et al., 2020; Zhang et al., 2021) for the same time period.

2.2.2 Global Dissimilarity and Constituency Analysis

To further identify geographical gaps in the coverage of the FLUXNET-CH4 Version 1.0 network, we quantified the dissimilarity of global wetlands from the tower network, using a similar approach to that taken for CO_2 flux towers (Meyer and Pebesma 2020). We calculated the 4-dimensional Euclidean distance from the four bioclimatic variables between every point at the land surface to every tower location at the FLUXNET-CH4 network. We then divided these distances by the average distance between towers to produce a dissimilarity index. Dissimilarity scores

<1 represent areas whose nearest tower is closer than the average distance among towers, while areas with scores >1 are more distant. Lastly, we identified the importance of an individual tower in the network by estimating the geographical area to which it is most analogous in bioclimate space. We divided the world's land surface according to closest towers in bioclimatic space. The area to which each tower is nearest is defined as the tower's constituency.

2.3 Wetland CH_4 seasonality

To examine freshwater wetland CH_4 seasonality across the global range of sites in FLUXNET-CH4, we extracted seasonality parameters for CH_4, temperature, and GPP using Timesat, a software package designed to analyze seasonality of environmental systems (Jönsson and Eklundh, 2002; Jönsson and Eklundh, 2004; Eklundh and Jönsson, 2015). Timesat calculates several seasonality parameters, including baseline flux, peak flux, and the slope of spring flux increase and fall decrease (Fig. 1). We also calculate parameters such as amplitude (peak flux - baseline, which is the average of spring and fall baselines; ("e" - (("a" + "b")/2) in Fig. 1), and relative peak timing (("g" - "f") / ("h" - "f") in Fig. 1). Timesat uses a double-logistic fitting function to create a series of localized fits centered on data minima and maxima. Localized fits are determined by minimizing ~~minimized using~~ a merit function ~~and~~ with the Levenberg-Marquardt method (Madsen et al., 2004; Nielsen, 1999). These localized fits are then merged using a global function to create a smooth fit over the full time interval. To fit CH_4 time-series in Timesat, we used gap-filled data after removing gaps exceeding two months. We do not report Timesat parameters when large gaps occur during CH_4 emissions spring increase, peak, or fall decrease.

We estimate 'start of elevated emissions season' when CH_4 emissions begin to increase in the spring ("f" in Fig. 1), and 'end of elevated emissions season' when the period of elevated CH_4 flux ends in the fall ("h" in Fig. 1), as the intercept between the Timesat fitted baseline parameter and shoulder-season slope (similar to Gu et al., 2009). To extract seasonality parameters with Timesat, sites need a sufficiently pronounced seasonality, a sufficiently long time period, and minimal data gaps (we note that while Timesat is capable of fitting two peaks per year, all the freshwater wetland sites have a single annual peak). We excluded site-years in restored wetlands when wetlands were still under construction. Of the 42 freshwater wetland sites in FLUXNET-CH4 Version 1.0, 36 had sufficient data series to extract seasonality parameters. These 36 wetlands had 141 site-years of data total, which we fit with the double-logistic fitting method which followed site data well (representative examples in Fig. 2). For extratropical sites in the Southern Hemisphere, we shifted all data by 182 days so that maximum solar insolation seasonality would be congruent across the globe.

We also used Timesat to extract seasonality metrics for GPP, partitioned using the daytime-based approach (Lasslop et al., 2010) (GPP_DT), air temperature (TA), and soil temperature (TS_1, TS_2, etc). For sites where winter soil temperatures fall significantly below 0 °C, Timesat fits a soil temperature "start of elevated season" date to periods when the soil is still frozen. In order for Timesat to define the soil temperature seasonality within the thawed season, we converted all negative soil temperatures to zero (simply removing these values results in too many missing values for Timesat to fit). Many sites have more than one soil temperature probe, so we extracted separate seasonality metrics from each individual probe (although we used the metrics from the shallowest temperature probe in our analysis). Tables B4 contain the Timesat seasonality parameters used in the seasonality analysis. We did not include water table depth in the seasonality analysis because many sites either lack water table depth measurements or have sparse data.

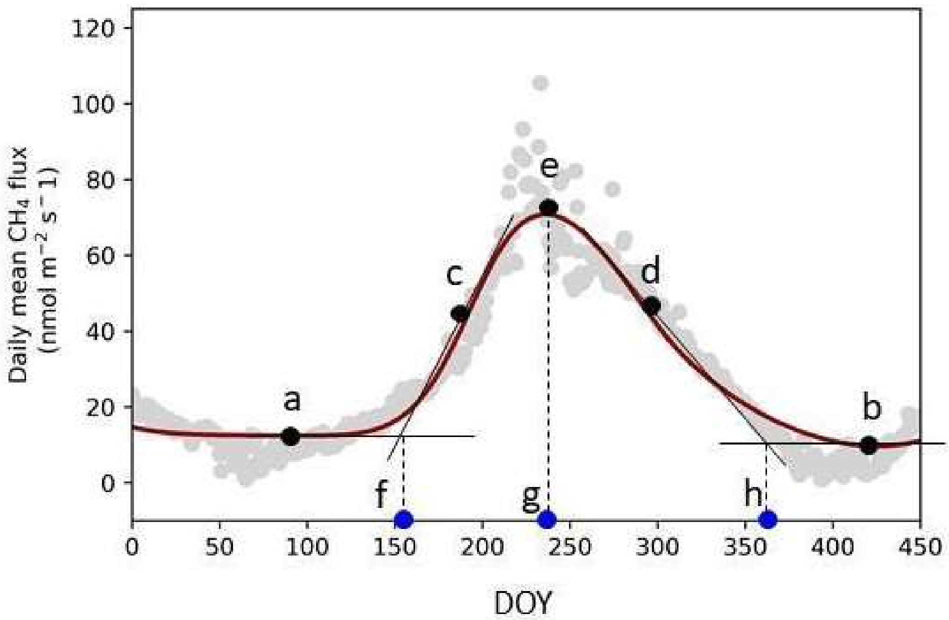

Figure 1: TIMESAT parameter description. (a) and (b) base values (Timesat reports the average of these two values), (c) and (d) slopes of seasonal curves (lines drawn between 20% and 80% of the amplitude), (e) peak value, and day of year (DOY) for the start (f), peak (g), and end (h) of the elevated methane (CH_4) emissions season. Data points are the mean daily gap-filled CH_4 fluxes from site JP-Bby in 2015.

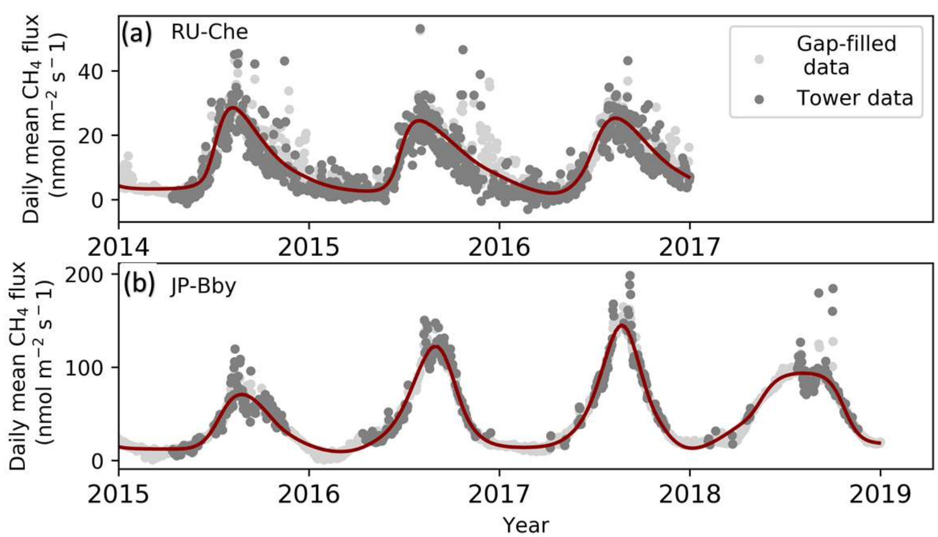

Figure 2: Examples of Timesat fits for two FLUXNET-CH4 sites, (a) RU-Che and (b) JP-Bby. Methane (CH_4) flux data showing daily average flux tower data, with several high outliers excluded to improve the plot (dark gray), gap-filled

values (light gray), and Timesat-fitted curve (dark red line) for sites JP-Bby and RU-Che. Timesat captures the size and shape of peaks (note different scale on y-axes). CH_4 = methane.

We regressed the CH_4 seasonality parameters from Timesat against annual temperature, annual water table depth, and Timesat seasonality parameters for air temperature, soil temperature, and GPP (proxy for recent carbon input available as substrate) using linear mixed-effect modeling with the *lmer* command (with site as a random effect) from the R (R Core Team 2018, version 3.6.2) package lmerTest (Kuznetsova et al., 2017). For these regressions we present the marginal R^2 outputs from *lmer*, which represent the variance explained only by the fixed effects. Mixed-effect modeling was necessary to account for the non-independence between measurements taken at the same site during different years (Zona et al., 2016; Treat et al., 2018). We also compared how seasonality metrics varied across latitudinal bands by dividing sites into northern (> 60° N), temperate (between 40° N and 60° N), subtropical (absolute value between 20° and 40° latitude, with site NZ-KOP being the only Southern hemisphere site), and tropical (absolute value below 20°). Site-year totals for the northern, temperate, subtropical, and tropical bands were n = 57, 36, 39, and 9, respectively. We used the Kruskal-Wallis test to establish whether groups (either across quarters or across latitudes) were from similar distributions, and the post hoc multiple comparison "Dwass, Steel, Critchlow, and Fligner" procedure for inter-group comparisons. Kruskal-Wallis and post-hoc tests were implemented in Python Version 3.7.4, using stats from scipy for Kruskal-Wallis and posthoc_dscf from scikit_posthocs.

We also compared quarterly CH_4 flux sums by dividing data into quarterly periods: January/February/March (JFM), April/May/June (AMJ), July/August/September (JAS), and October/November/December (OND). For the sake of simplicity, we chose to compare quarterly periods rather than site-specific growing/non-growing season periods so that all time periods would be the same length. Quarterly sums were computed from the gap-filled CH_4 fluxes when the longest continuous data gap within the quarter did not exceed 30 days, leading to site-year counts of 67, 92, 95, 72 for JFM, AMJ, JAS, and OND, respectively. We compared quarterly CH_4 fluxes across latitudinal bands both for the total CH_4 flux, and for the quarterly percentage of the annual CH_4 flux. Quarterly statistics were also conducted with the Kruskal-Wallis test and the post hoc multiple comparison "Dwass, Steel, Critchlow, and Fligner" procedure implemented in Python. Quarterly values are provided in Table B3, and the sum of mean quarterly CH_4 flux does not always equal mean annual CH_4 flux because some quarters either do not have data, or have data gaps that exceed 30 days.

3. Results and Discussion

3.1 FLUXNET-CH4 dataset

3.1.1 Dataset description

Version 1.0 of the FLUXNET-CH4 dataset contains 79 unique sites, 293 total site-years of data, and 201 site-years with sufficient data to estimate annual CH_4 emissions. A synthesis paper, published prior to the public data release of FLUXNET-CH4 Version 1.0, had 60 unique sites and 139 site-years with annual CH_4 emissions estimates (Knox et al., 2019). Freshwater wetlands make up the majority of sites (n = 42), and the dataset also includes five salt marshes and one mangrove wetland. Notable additions to FLUXNET-CH4 from the previous unpublished dataset used in Knox et al., (2019) include six tropical sites (between 20° S and 20° N), including one site in South America, two sites in southern Africa, and three sites in Southeast Asia. The 15 upland sites include six needleleaf forests, three crop sites (excluding rice), two alpine meadows, one grassland, one mixed forest, one tundra, and one urban site. The drained sites represent former wetlands that have been artificially drained for use as grasslands (n = 3) or croplands (*n* = 3). FLUXNET-CH4 sites span the globe, though are concentrated in North America and Europe (Fig. 3). Table B3 includes characteristics of all sites in the dataset.

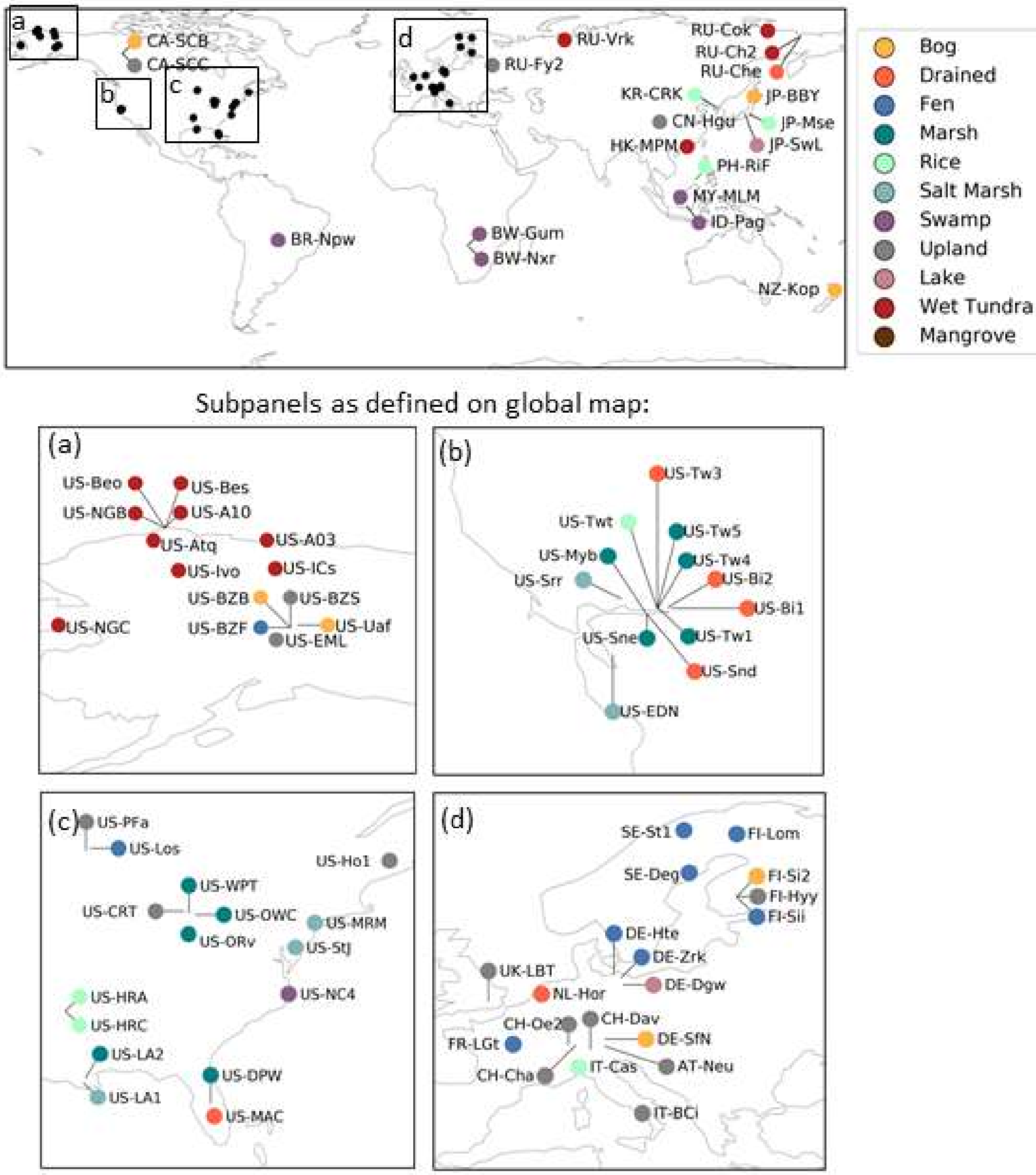

Figure 3. Global map of FLUXNET-CH4 Version 1.0 site locations colored by site type. Insets (a)-(d) show sites that were too closely located to distinguish in the global map.

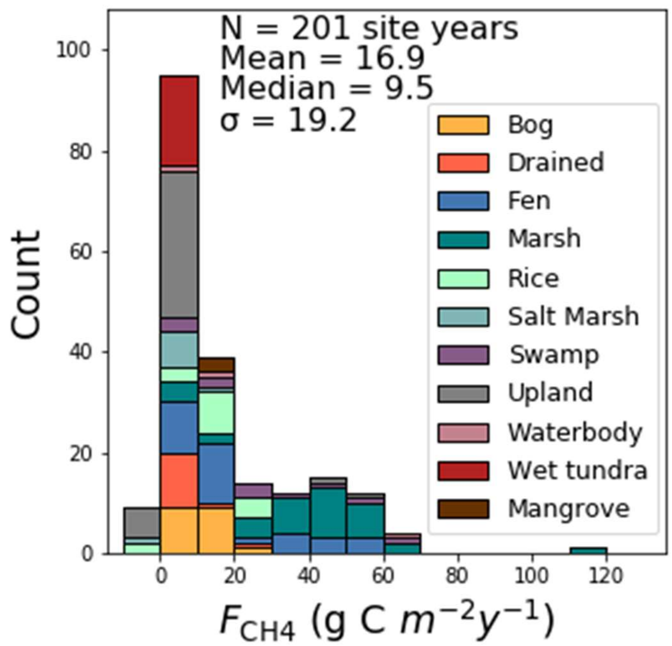

Figure 4. Histogram of annual methane fluxes (F_{CH4}, g C m^{-2} yr^{-1}) grouped by site type.

Sites represent a range of ecosystem types, latitudes, median fluxes, and seasonality patterns (Table 1). Across all FLUXNET-CH4 sites (including non-wetland sites), mean average annual CH_4 flux is positively skewed with a median flux of 9.5 g C m^{-2} yr^{-1}, a mean flux of 16.9 g C m^{-2} yr^{-1}, and numerous annual CH_4 fluxes exceeding 60 g C m^{-2} yr^{-1}. Marshes and swamps have the highest median flux, and upland, salt marsh, and tundra sites have the lowest (Fig. 4). Lake emissions are highly variable due to one high-flux lake site (JP-SWL). Flux data at many sites show strong seasonality in CH_4 emissions, but data coverage is also lower outside the growing season (Table 1). Data coverage is lowest during the JFM quarter (on average 20% of half-hourly time periods contain flux data) reflecting the predominance of Northern hemisphere sites and the practical difficulties in maintaining EC tower sites during colder winter months (Table 1). Bogs, fens, and marshes have pronounced seasonality, with fluxes being highest in the AMJ and JAS quarters. In contrast, CH_4 fluxes from uplands, drained sites, and salt marshes are more uniform and low year-round.

Table 1: Summary table of sites grouped by ecosystem class reporting annual mean flux (Ann_Flux) and standard deviation from inter-annual variability (Ann_Flux_SD), site-years of data, % data cover per quarter, and median (med.) flux across site class. JFM= January, February, March; AMJ = April, May, June; JAS = July, August, September; OND = October, November, December.

	# of Sites	# of Site-Years	Ann_Flux g C m^{-2} $year^{-1}$	Ann_Flux_SD g C m^{-2} $year^{-1}$	JFM cover-age (%)	AMJ cover-age (%)	JAS cover-age (%)	OND cover-age (%)	JFM flux (med.)	AMJ flux (med.)	JAS flux (med.)	OND flux (med.)
Salt marsh	5	10	2.9	4.7	7	42	50	37	1.5	1.7	2.1	1.6
Wet tundra	11	39	3.8	1.8	8	28	40	18	0.4	2.6	8.1	3.2

Upland	15	47	4.0	10.5	23	35	39	28	1.2	0.5	1.4	0.8
Drained	7	20	6.3	7.1	22	39	39	29	4.6	3.6	5.1	3.6
Bog	7	32	10.5	6.4	8	27	37	18	7.2	11.0	24.8	9.5
Mangrove	1	3	11.1	0.5	46	28	30	41	3.2	7.2	22.5	14.1
Rice	7	20	14.4	8.8	16	37	45	27	3.2	11.9	43.1	4.2
Fen	8	40	20.5	16.0	29	43	40	30	2.8	14.2	26.0	6.4
Swamp	6	15	26.4	19.9	24	34	29	19	14.7	24.9	31.0	24.4
Lake	2	4	28.2	33.4	15	13	27	36	0.2	47.6	90.2	40.3
Marsh	10	42	40.8	20.7	22	43	53	30	13.5	55.0	85.8	36.1

3.1.2 Freshwater wetland CH_4 characteristics

The FLUXNET-CH4 Version 1.0 dataset contains 42 freshwater wetlands that span 37°S to 69°N, including bogs, fens, wet tundra, marshes, and swamps, and a range of annual CH_4 emission rates (Fig. 4). The majority of freshwater wetlands in our dataset emit 0-20 g C m^{-2} yr^{-1}, with 10 emitting 20-60 g C m^{-2} yr^{-1}, and one more than 60 g C m^{-2} yr^{-1}. Differences in annual CH_4 flux among wetland types is partially driven by temperature (which is often linked to site type), with mean annual air temperature explaining 51% of the variance between sites (Fig. 5, exponential relationship). The global relationship between annual methane emissions and temperature can be described using a Q_{10} relationship where $Q_{10} = R2/R1^{((T2-T1)/10)}$, with R2 and R1 being the CH_4 emission rates at temperatures T2 and T1, respectively (temperature in degrees C). The Q_{10} based on Fig. 5 data is 2.57. We also note that annual CH_4 flux from individual biomes may have different relationships with temperature, as previous work has shown biome-specific trends in CH_4 flux with environmental drivers (Abdalla et al., 2016). However, there currently are not enough data points in each biome category to compare relationships between mean annual CH_4 flux and temperature. Annual CH_4 flux is not correlated with mean annual water table depth in FLUXNET-CH4, unlike in Knox et al., (2019), which used a subset of the FLUXNET-CH4 sites where CH_4 flux was correlated with water table depth only for sites with water table below ground for 90% of measured days ($r^2 = 0.31$, $p<0.05$, $n = 27$ site years). Freshwater wetland seasonality is further described in Sect. 3.3.

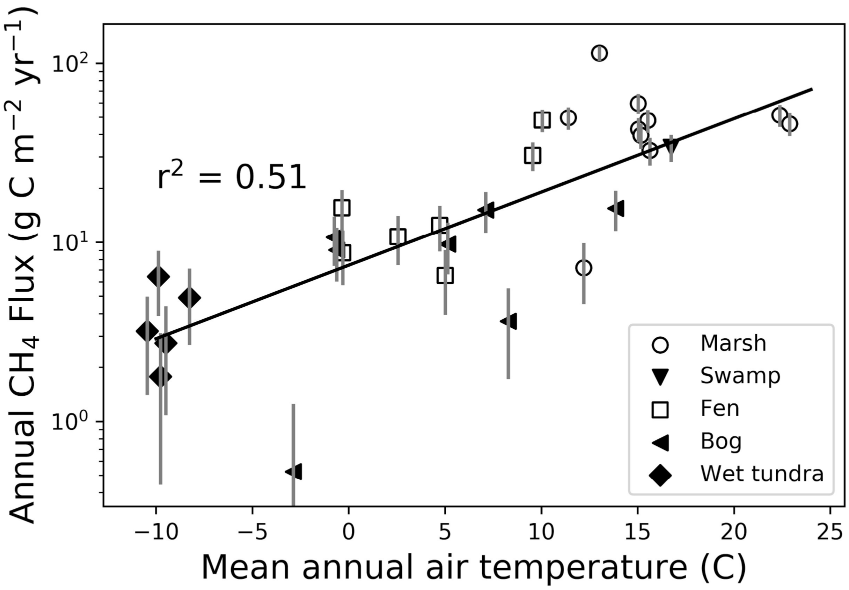

Figure 5: Relationship between mean annual wetland methane (CH_4) flux (g C m^{-2} yr^{-1}, logarithmic scale) and mean annual air temperature (°C) for each freshwater wetland site, with wetland type indicated by symbol. Markers represent individual site means, with vertical error bars representing the standard deviation of interannual variability.

3.1.3 Upland, rice and urban CH_4 characteristics

Upland agricultural sites are characterized by a lack of seasonal pattern in CH_4 emissions, relatively low flux, and sometimes negative daily flux (i.e., CH_4 uptake) averages. All of the upland non-agricultural sites in FLUXNET-CH4 Version 1.0 are net (albeit weak) CH_4 sources except for the needleleaf forest site US-Ho1, which has mean annual CH_4 flux of -0.1 ± 0.1 g C m^{-2} yr^{-1} (see Table B3 for site acronyms and metadata). The average agricultural site emissions are 1.3 ± 0.8 g C m^{-2} yr^{-1} and non-agricultural site emissions are 1.6 ± 1.2 g C m^{-2} yr^{-1} across sites.

Rice sites (n = 7) have average annual emissions across all sites of 16.7 ± 7.7 g C m^{-2} yr^{-1} and are characterized by strong seasonal patterns, with either one or more CH_4 emission peaks per year depending on the number of rice seasons and field water management. One peak is typically observed during the reproductive period for the continuously flooded sites with one rice season (i.e., US-HRC, JP-MSE) (Iwata et al., 2018; Runkle et al., 2019; Hwang et al., 2020). For sites with only one rice season but with single or multiple drainage and re-flooding periods, a secondary peak may appear before the reproductive peak (i.e., KR-CRK, IT-Cas, and US-HRA; Meijide et al., 2011; Runkle et al., 2019; Hwang et al., 2020). Two reproductive peaks appear for sites with two rice seasons (i.e., PH-RiF), and each reproductive peak may be accompanied by a secondary peak due to drainage events (Alberto et al., 2015). Even sites with one, continuously flooded rice season may experience a second peak if the field is flooded during the fallow season to provide habitat for migrating birds (e.g., US-Twt; Knox et al., 2016).

The dataset has one year of urban data from site UK-LBT in London, England. UK-LBT observes CH_4 fluxes from a 190 m tall communications tower in the center of London, and has a mean annual CH_4 flux of 46.5 ± 5.6 g C m^{-2} yr^{-1}. This flux is more than twice as high as the mean annual CH_4 flux across all FLUXNET-CH4 sites, 16.9 g C m^{-2} yr^{-1}. The London site has higher CH_4 emissions in the winter compared to summer, which is attributed to a seasonal increase in natural gas usage (Helfter et al., 2016.)

3.1.4 Saltwater and mangrove wetland CH_4 characteristics

Three of the five saltwater wetlands in FLUXNET-CH4 (US-Edn, US-MRM, and US-Srr) have a very low mean annual CH_4 flux (see Table B2 for individual site-year CH_4 flux sums and associated uncertainty) and minimal seasonality. Two other FLUXNET-CH4 saltwater sites (US-La1 and US-StJ) have significantly higher fluxes, with annual sums of 12.6 ± 0.6 and 9.6 ± 1.0 g C m^{-2} yr^{-1}, respectively, while the mangrove site HK-MPM has annual mean fluxes of 11.1 ± 0.5 g C m^{-2} yr^{-1}. This range of CH_4 fluxes across different saltwater ecosystems could be valuable for exploring the effect of salinity and different biogeochemical pathways of CH_4 production, oxidation, and transport of CH_4 (Bartlett et al., 1987; Poffenbarger et al., 2011). Saltwater wetlands along the coast have unique CH_4 dynamics attributable to the presence of abundant electron acceptors, most importantly sulphates, which inhibit methanogenesis (Pattnaik et al., 2000; Mishra et al., 2003; Weston et al., 2006), but at low concentrations can have no effect (Chambers et al., 2011) or even increase methanogenesis (Weston et al., 2011). In fact, estuarine wetlands with moderate salinity can still be significant sources of CH_4 (Liu et al., 2020). Even under sulfate-rich conditions, high CH_4 production can be found via methylotrophic methanogenesis (Dalcin Martins et al. 2017; Seyfferth et al., 2020,) or because the processes of sulfate reduction and methanogenesis are spatially separated (Koebsch et al., 2019). Consequently, representing the biophysical drivers of ecosystem-scale CH_4 fluxes in non-freshwater wetlands is challenging and may represent a combination of competing or confounding effects (Vazquez-Lule and Vargas 2021).

3.2 Freshwater w~~W~~etland r~~R~~epresentativeness

We evaluated the representativeness of freshwater wetland sites in the FLUXNET-CH4 Version 1.0 dataset against wetlands globally, based on bioclimatic conditions of our sites. When evaluating bioclimatic variables individually, the distribution of freshwater wetlands across the network was significantly different from the global distribution (alpha > 0.05; two-tailed Kolmogorov-Smirnov tests; see Table B4). We exclude wetlands classified as "Salt Marsh" in this representativeness analysis and the seasonality analysis below because of the unique CH_4 flux dynamics in saltwater ecosystems (as discussed in section 3.1.4), though we note that some of the coastal wetlands included in the freshwater analysis periodically experience brackish water (i.e.: US-Myb, US-Sne).

When considering the four bioclimatic variables, MAT, LE, EVI and SRWI in a PCA, we found that our tower network generally samples the bioclimatic conditions of global wetland cover, but some noticeable gaps remain (Fig. 6). Three clusters of the world's wetland-dense regions are identified, but are not equally sampled by the network. A cluster of low temperature wetlands is sampled by a large number of high-latitude sites. The other two wetland clusters are not as well sampled: a high temperature and LE cluster is represented only by two towers (ID-Pag and MY-MLM), while drier and temperate and subtropical wetlands including large swathes of the Sahel in Africa only have a site in Botswana (BW-Npw) as their closest-analog tower.

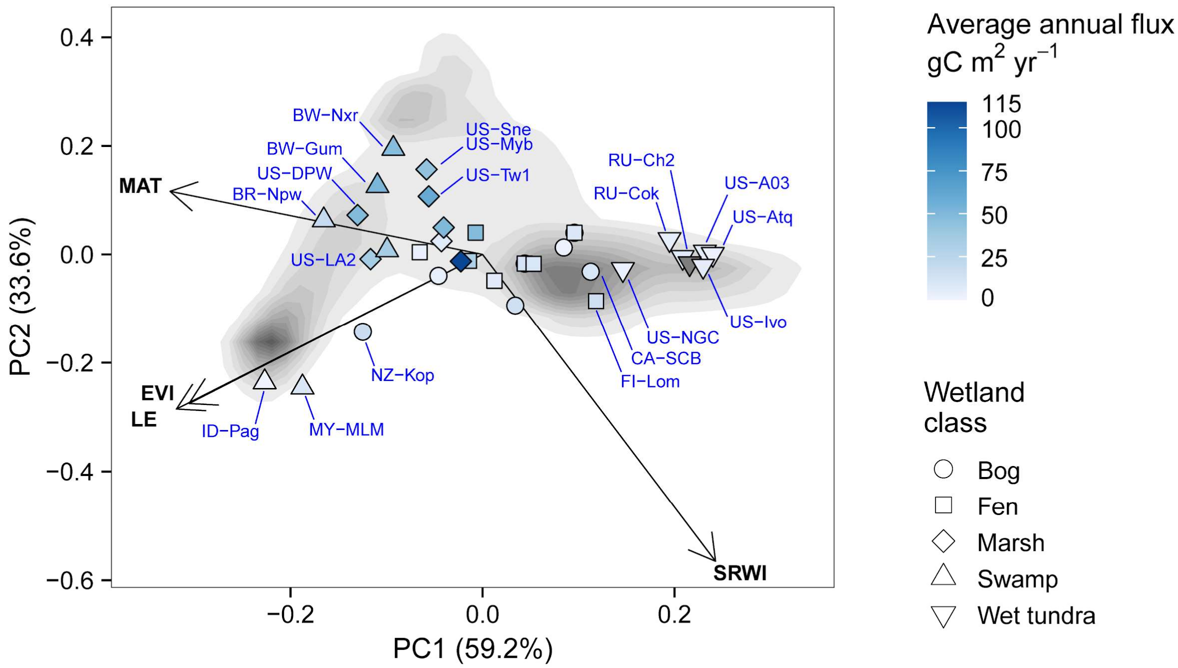

Figure 6: Principal Component Analysis displaying the distribution of freshwater wetland sites (points) along the two main principal components together accounting for 91.9% of variance. Tower sites are represented as points with shapes indicating their wetland type and color shade representing the annual methane (CH_4) flux (gray points represent sites for which <6 months of flux data was available to estimate annual budget). Sites codes are labeled in blue text for selected sites deviating from average conditions. Loading variables are represented by the arrows: mean annual temperature (MAT), simple ratio water index (SRWI), latent heat flux (LE) and enhanced vegetation index (EVI). The background shades of gray are a qualitative representation of the density of global wetland pixels and their distribution in the PCA climate-space, with darker color representing higher densities (excluding Greenland and Antarctica). Only grid cells with >5% average wetland fraction according to the WAD2M over 2000-2018 are included (Zhang et al., 2020). The loading variables are represented by the arrows: mean annual temperature (MAT), simple ratio water index (SRWI), latent heat flux (LE) and enhanced vegetation index (EVI).

Evaluating the bioclimatic dissimilarity of global wetlands to the FLUXNET-CH4 network shows the least captured regions are in the tropics (Fig. 7A). Sparse coverage in the tropics also means that the few existing towers occupy a critical place in the network, particularly as tropical wetlands are the largest CH_4 emitters (Bloom et al., 2017; Poulter et al., 2017). Highly dissimilar wetlands are limited in extent and distributed across all latitudes, but the average dissimilarity is higher in north temperate (55° to 65°) and tropical (-5° to 5°) latitudes (Fig. 7B). To evaluate the importance of individual towers in the network, we estimated the geographical area to which it is most analogous in bioclimate-space (Fig. 7C). We found that some towers have disproportionately large constituencies (i.e., wetland areas that share the same closest bioclimatic analog tower). Towers in Indonesia (ID-Pag), Brazilian Pantanal (BR-Npw), and Botswana floodplains (BW-Nxr) represent the closest climate analog for much of the tropics (678, 300 and 284 thousand km^2, respectively) while CA-SCB represents a vast swath (291 thousand km^2) of boreal/arctic regions (Fig. 7D).

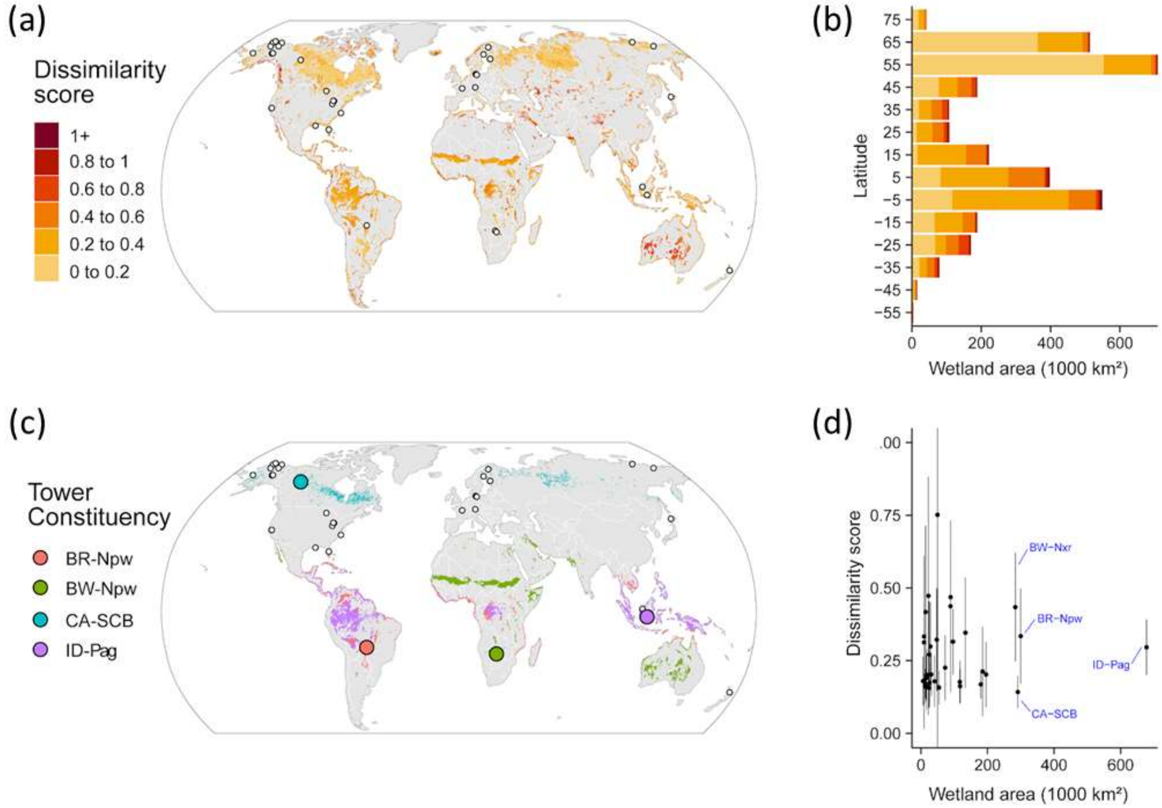

Figure 7: (a) Distance in bioclimatic space between global land surface and the FLUXNET-CH4 Version 1.0 tower network (gray areas indicate no mapped wetlands). The Euclidean distance was computed on the four bioclimatic variables and was then standardized by the average distance within-network. Most of the land surface has a dissimilarity score lower than 1, meaning these areas are closer than the average tower distance (lower dissimilarity score means a similar bioclimate to that represented by towers in the network). However, this pattern reflects more the sparsity of the tower network than a similarity of the land surface to the network. Areas with <5% coverage by wetlands were excluded to focus on wetland-dense regions. (b) Latitudinal distribution of dissimilarity score, (c) Map of the four largest tower constituencies, (d) Scatterplot of wetland area in each tower constituency plotted against the average dissimilarity score (point) and +/- standard deviation (error bar).

Our assessment of wetland CH_4 tower coverage determines the ability of our dataset to represent global wetland distributions and highlights some clear representation gaps in the network, particularly in tropical and humid regions. Other geographic regions such India, China, and Australia, where towers exist but are not included in the current network should be prioritized when expanding the network, even though they are not among the most distant areas to the current network. Similar representativeness assessments have been developed for CO_2 tower networks to identify gaps and priorities for expansion (Jung et al., 2009). To improve the geographic coverage of the network for representing global-scale fluxes, locations for new tower sites can be targeted to cover bio-climatically distant areas from the current network (Villarreal et al., 2019). Candidate regions for expansion that are both high CH_4 emitting (Saunois et al., 2020) as well as located in under-sampled climates are: African Sahel, Amazon basin, Congo basin, South-East Asia. Climatic conditions over boreal and arctic biomes are generally better represented (primarily at lower elevations), but there is scope to expand the network in wetland-dense regions like the Hudson Bay Lowlands and Northern Siberian Lowlands. Moreover, establishing sites in other ecosystem types, especially lakes and reservoirs (see Deemer et al. 2016, Bastviken et al. 2011, Matthews et al. 2020) in most climatic zones would help capture CH_4 fluxes from these ecosystems.

Understanding the representativeness of the network is essential when inferring general patterns of flux magnitude, seasonality, and drivers from the tower data (Villarreal et al., 2018). We produced a first-order representativeness of average bioclimatic conditions, but temporal representativeness (across seasons, climate anomalies and extreme events) is particularly needed given the episodic nature of CH_4 fluxes (Chu et al., 2017; Mahecha et al., 2017; Göckede et al., 2019).

Assessing representation of wetland CH_4 sites is complicated by the fact that wetlands occupy only a fraction of most landscapes (except wetland dense regions such as Northern Siberian Lowlands, Hudson Bay Lowlands, Congo basin, etc.) and that not all relevant factors affecting CH_4 production and consumption could be considered in our analysis. For instance, our assessment of representation did not consider wetland types as such maps are limited by the inherent difficulties in remotely sensing wetland features (Gallant, 2015). The attribution of representativeness is further complicated by the fact that many EC tower locations are subject to small-scale variability within the field of view, or footprint, of the sensor. Consequently, the individual time steps within EC flux time series may represent a mixture of different wetland types, or different fractions of wetland contribution to the total CH_4 flux, varying with wind direction, atmospheric stability, or season (Chu et al 2021). This further complicates upscaling efforts. Additionally, this representativeness analysis did not apply weights to the drivers to reflect their varying influence on CH_4 flux. Such weights can be included in future versions as they are generated by a cross-validated machine learning approach (Jung et al., 2020). Future efforts could include the dissimilarity index from this analysis as a metric of extrapolation in a CH_4 flux upscaling effort.

3.3 Freshwater wetland flux seasonality

3.3.1 Seasonal flux comparisons by latitudinal bands

CH_4 flux and seasonality varied substantially across latitudinal bands (northern, temperate, subtropical, and tropical) (Fig. 8). Annual CH_4 fluxes for temperate, and subtropical sites were significantly higher than for northern sites (8.7 ± 5.0, 29.7 ± 25.2, 40.1 ± 14.6, and 24.5 ± 20.7 g C m^{-2} yr^{-1} for northern, temperate, subtropical, and tropical, respectively, $p<0.0001$ using Kruskal Wallis and post hoc comparisons; Fig. 8a), and tropical sites were similar to all other latitudinal bands likely because of their small sample size. The ratio of seasonal amplitude to peak flux provides a measure of the relative seasonal increase in emissions compared with baseline, where a ratio of zero indicates no seasonal change in amplitude, a ratio of one indicates the off-season flux is zero, and values over one means the off-season baseline CH_4 fluxes were negative (i.e., uptake). Average amplitude to peak flux ratios were similar across all latitudinal bands (0.9 ± 0.1, 0.9 ± 0.1, 0.9 ± 0.1, 1.0 ± 0.7, for northern, temperate, subtropical, and tropical, respectively; Fig. 8b). The spring increase in CH_4 emissions began later in northern sites compared with temperate and subtropical sites (end of May versus April, respectively, $p=0.001$; Fig. 8c), while tropical sites vary widely in elevated emission season start date. Northern sites also had shorter elevated CH_4 flux season lengths (138 ± 24 days) compared to temperate sites (162 ± 32 days), and both were shorter than subtropical sites (209 ± 43 days; $p<0.0001$; Fig. 8e). On average, CH_4 flux peaked earlier for temperate sites compared to northern ($p = 0.008$) and subtropical sites ($p = 0.02$; mid to late July compared with early August; Fig. 8f), while tropical sites again vary widely. Given their unique seasonality, and low number of site-years ($n = 9$), tropical systems are discussed separately in Sect. 3.3.3, and not included in the comparisons in the remainder of this section. While our results on CH_4 seasonality corroborate expected trends for these latitudinal bands, they provide some of the first estimates of CH_4 seasonality parameters and ranges across a global distribution of sites.

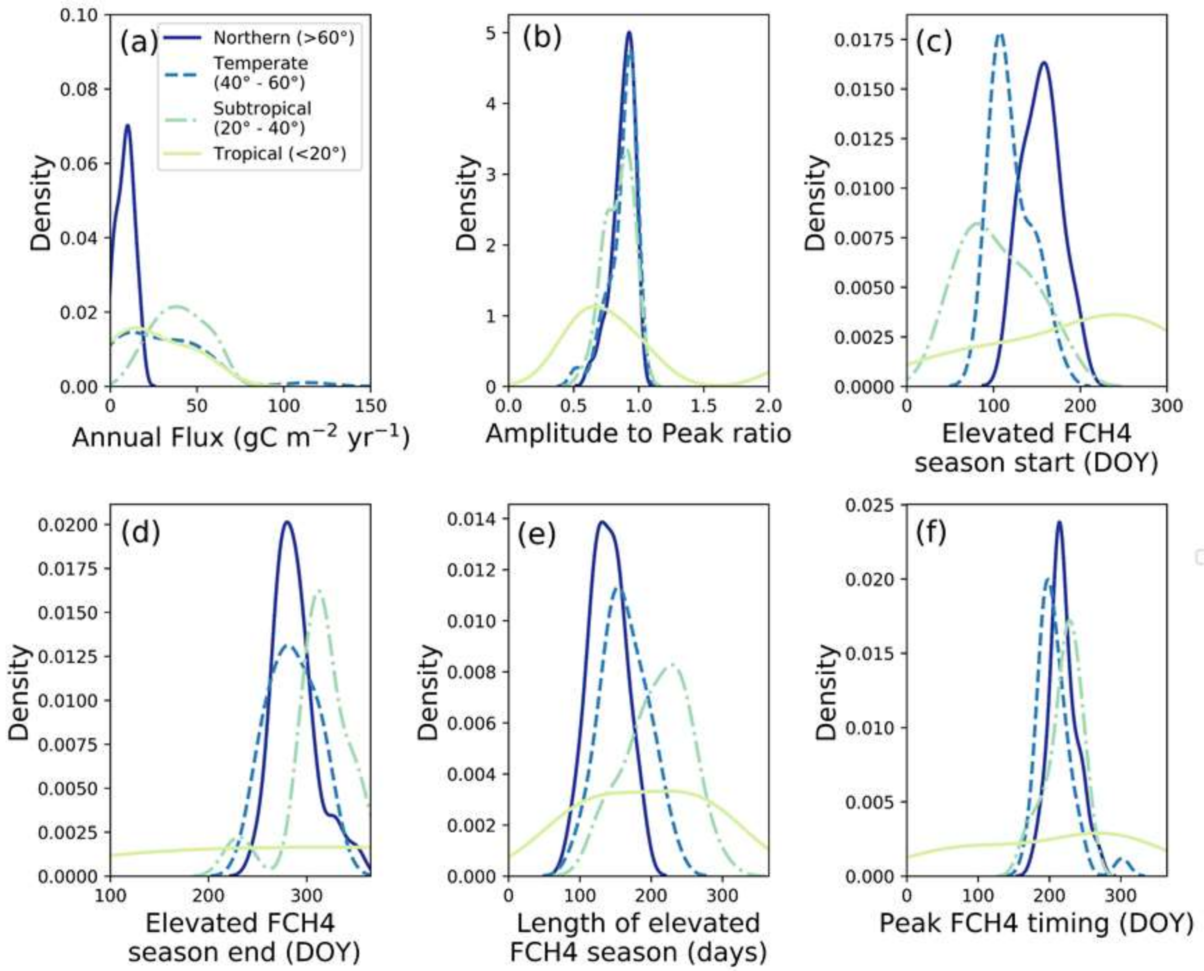

Figure 8: (a) Annual methane (CH_4) flux (g C m^{-2} yr^{-1}), (b) Ratio of seasonal amplitude to seasonal peak, where values of 0 indicate uniform annual CH_4 flux, values of one indicate zero off-season fluxes, and values exceeding one indicate negative off-season fluxes, (c) CH_4 flux (FCH4) elevated emissions season start by day of year (DOY), (d) FCH4 elevated emissions season end by DOY, (e) Length of elevated CH_4 flux season (days), and (f) DOY of peak FCH_4. Northern (dark blue, solid line), Temperate (blue, dashed line), Sub-tropical (green, dot-dash line) and Tropical (light green, solid line) wetlands plotted using the kernel density function. Each panel has lines that represent latitudinal bands as follows: northern (> 60°), temperate (between 40° and 60°), subtropical (between 20° and 40°), and tropical (< 20°), though the site-year totals vary between these groups (n = 57, n = 36, n = 39, and n = 9 respectively). All total CH_4 flux values and elevated season start values are positive, and the apparent continuation of the data distribution into negative values is an artifact of the kernel density function. Southern Hemisphere sites below 20° S were shifted by 182 days to make summer the middle of the year for comparability with Northern Hemisphere sites.

We found that latitudinal groups showed strong differences in absolute CH_4 flux across quarters, and narrower differences in percentage of annual CH_4 flux (Fig. 9a versus 9b). Thus, the AMJ quarter had a similar relative contribution to the annual CH_4 flux across latitudes, regardless of the absolute annual CH_4 flux. CH_4 fluxes (Fig. 9a) were highest during JAS for northern, temperate, and subtropical sites and highest in AMJ and JAS for temperate sites ($p<0.01$). Though CH_4 fluxes in northern sites are most commonly measured during warm summer months (Sachs et al., 2010; Parmentier et al., 2011), fluxes in JFM and OND (50% of the yearly duration) on average make up 18.1 ± 3.6%, 15.3 ± 0.1%, and 31.2 ± 0.1% (northern, temperate, subtropical, respectively) of annual emissions. This pattern indicates that a substantial fraction of annual CH_4 fluxes occurs during cooler months. The contribution of nongrowing season CH_4 emissions to annual CH_4 fluxes has previously been described for arctic and boreal regions (Zona et al., 2016; Treat et al., 2018) and our analysis suggests comparable contributions in temperate and subtropical systems for the same quarterly periods.

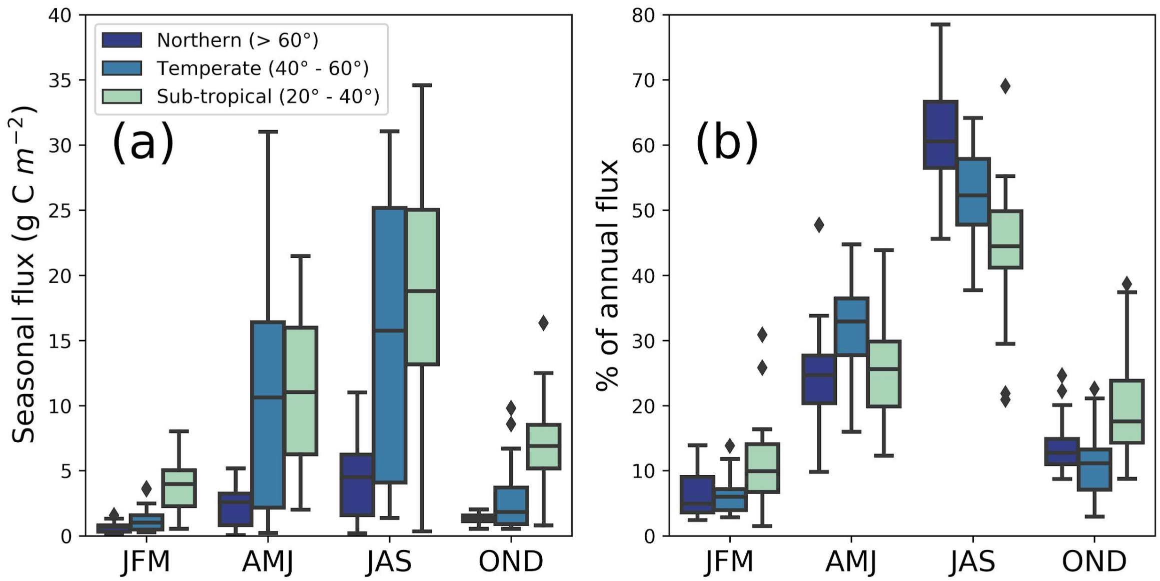

Figure 9: (a) Quarterly contribution to total annual CH_4 flux in g C m^{-2}, and (b) percentage of annual CH_4 flux. Sites were divided into northern (> 60° N), temperate (40° N - 60° N), and subtropical (20° N - 40° N). Quarters with continuous data gaps exceeding 30 days were excluded. We used the following quarterly periods: January/February/March (JFM), April/May/June (AMJ), July/August/September (JAS), and October/November/December (OND). Tropical sites are discussed separately in Sect. 3.3.3 because of their unique seasonality and low number of sites.

3.3.2 Predictors of CH_4 flux phenology

The start of the elevated CH_4 flux season, and how long the elevated flux season lasts, correlated strongly with mean annual air temperature (Fig. 10; $p<0.0001$ for each). Methane flux began to increase roughly two months earlier in the warmest systems (mean annual temperature > 20 °C) compared to the coldest (mean annual temperature near -10 °C), though several of the warmer sites had high variability. Our data suggest that the CH_4 season started 2.8 ± 0.5 days earlier for every degree Celsius increase in mean annual temperature (Fig. 10a). In contrast, the end of the CH_4 emission season was not correlated with mean annual temperature, but a positive trend existed despite high variability in warmest and coldest sites (Fig. 10b). The high variability seen in the end of CH_4 season at northern sites is important to note and would likely be better resolved by incorporating other seasonality or phenological characteristics, such as moisture, active layer depth, and plant community composition (e.g., Kittler et al., 2017). Plants with aerenchymatous tissue, for example, influence the timing of plant-mediated CH_4 flux and are a key source of uncertainty while predicting CH_4 seasonality for northern wetlands (Xu et al., 2016, Kwon et al., 2017). Despite the relative lack of trend with season end date, the season length was still positively correlated with mean annual temperature, with the warmest sites having roughly three more months of seasonally elevated CH_4 emissions than the coldest sites (Fig. 10c). CH_4 season length increased 3.6 ± 0.6 days for every degree Celsius increase in mean annual temperature (note that these relationships are correlations, and we cannot disentangle causality with this analysis). Temperature is highly correlated with other parameters (i.e., radiation, days of snow cover, etc.), so CH_4 flux is also likely to correlate with other environmental parameters.

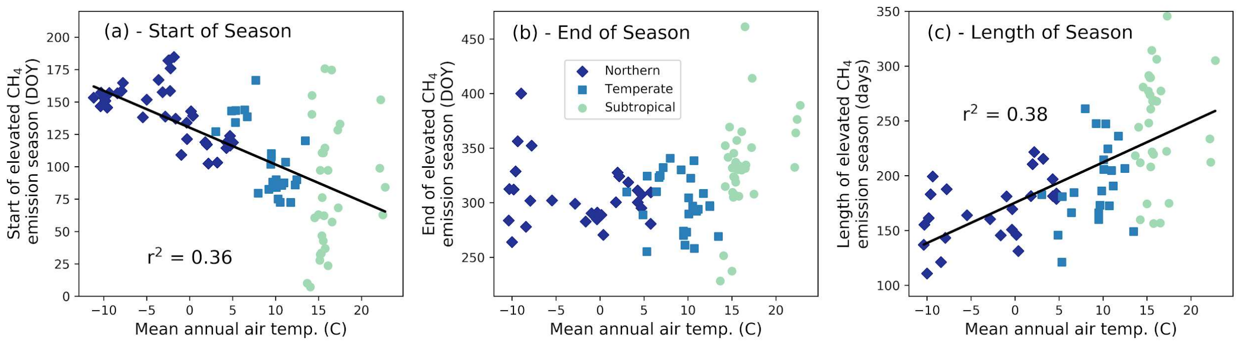

Figure 10. The (a) start of the elevated methane (CH_4) emission season (y = -2.8x + 130, with 'x' in °C and 'y' in day of year (DOY)), (b) the end of the elevated emission season in DOY, and (c) the length of the emission season with mean annual site air temperature (y = 3.6x + 176.6, with 'x' in °C and 'y' in days). Each point represents a site-year of data and all reported r^2 are significant to $p < 0.0001$. Tropical sites are discussed separately in Sect. 3.3.3.

Although the spring onset of increasing CH_4 emissions correlated with mean annual air temperature, on average it lagged the spring increase in the shallowest soil temperatures by 31 ± 40 days (Fig. 11, lag is significantly different than zero, $p < 0.001$), with very few instances of CH_4 emissions beginning before seasonal soil temperatures increase (and by 20 ± 50 days for the deepest temperature probes). In contrast, for roughly half of the sites, CH_4 emission increased prior to seasonal GPP (a proxy for fresh substrate availability) increases. This suggests that the initiation of increased CH_4 fluxes at the beginning of the season was not limited by availability of substrate derived from recent photosynthate. Additionally, the onset of CH_4 fluxes tended to occur closer to the onset of soil temperature increase for cooler temperature sites (sites with later start dates tend to be cooler; Fig. 11a). This result is likely attributable to the direct influence of increased temperature on microbial processes (Chadburn et al., 2020), as well as the indirect influences of snow melt, both via release of CH_4 from the snowpack as well as a higher water table leading to more CH_4 production (Hargreaves et al., 2001; Tagesson et al., 2012; Mastepanov et al., 2013; Helbig et al., 2017). These observed trends hold for the entire temperature or GPP range of freshwater wetland sites, but are not necessarily applicable within individual latitudinal bands.

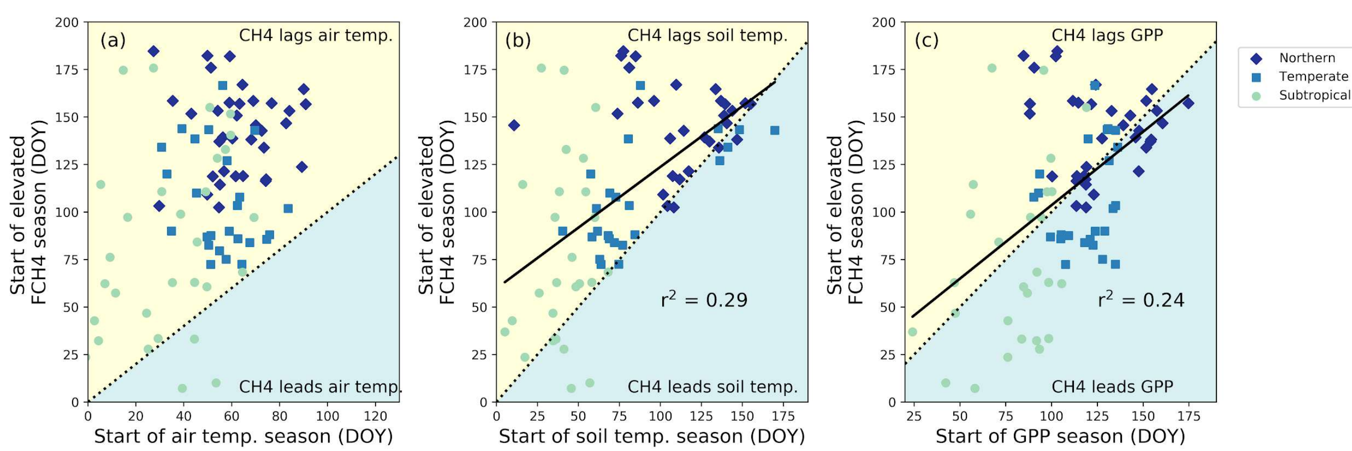

Figure 11. Relationship between the onset of the onset of the methane (CH_4) emission season to (a) the beginning of the air warming by day of year (DOY), (b) soil warming at the shallowest probe depth per site by DOY, and (c) gross primary productivity (GPP) increase for the subset of sites with soil temperature data by DOY. Each point represents a site-year of data. Dashed lines represent a 1:1 relationship, solid lines are significant ($p < 0.05$) regression fits. On average, the CH_4 emission season lags the soil temperature increase by 31 ± 40 days, and is more synchronous with GPP.

In contrast with the CH_4 season-start timing, the timing of the CH_4 peak did not correlate with either the timing of the soil temperature peak or the GPP peak (Fig. A1). For 63% of the sites, the average timing of peak CH_4 emissions lagged the soil temperature peak, and at 83% of the sites average peak CH_4 lagged peak GPP (Fig. A1). Although there was no simple relationship between absolute CH_4 peak timing and the environmental drivers we investigated, there was a correlation ($p = 0.0005$) between the relative timing of peak CH_4 compared to season onset (calculated as described in Section 2.3) and mean annual air temperature (Fig. 12a). For cooler sites, the peak of seasonal CH_4 emissions occurred closer to the onset of the CH_4 emission season than the end of the season, resulting in an asymmetrical seasonal CH_4 flux shape that is illustrated in Fig. 2a. Soil temperature also peaked earlier in the season for cooler wetlands, though the relationship is not as pronounced ($p = 0.009$, Fig. 12b). In contrast, GPP peaked later in the season for cooler wetlands ($p = 0.009$, Fig. 12c). Previous work on Arctic sites (sites US-Ivo, US-Beo, US-Atq, US-Bes, and RU-CH2) highlighted the asymmetrical annual CH_4 peak, with higher fall emissions being attributed to the "zero curtain" period when soil below the surface remains thawed for an extended period of time due to snow insulation (Zona et al., 2016; Kittler et al., 2017). Furthermore, soils can stay above the "zero curtain" range for an extended time into the fall and winter (Helbig et al., 2017), which may also be caused by snow insulation. The rapid onset of emissions in the spring following snowmelt could be attributed to the release of accumulated CH_4 (Friborg et al., 1997), and other high latitude sites have seen similarly sharp increases in CH_4 emissions at snowmelt (Dise, 1992, Windsor, 1992). However, not all studies in high latitudes have observed asymmetrical CH_4 emission peaks, pointing to the inherent complexity of these ecosystems (Rinne et al., 2007; Tagesson et al., 2012).

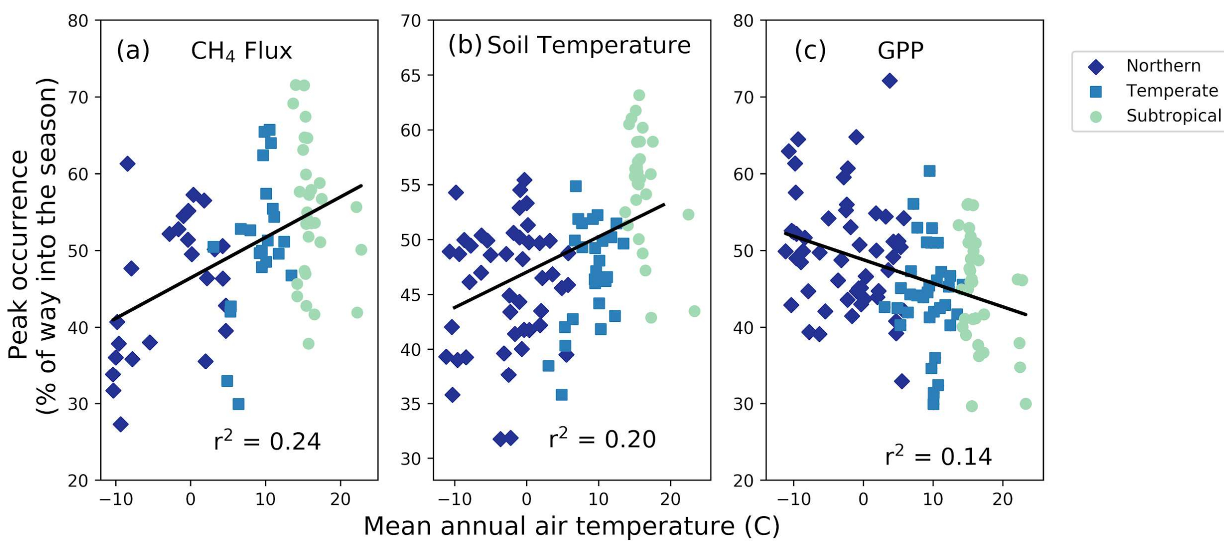

Figure 12. Site-year peak methane (CH_4) emission (a) and peak soil temperature (b) occur earlier in the season for sites with lower mean annual temperatures. (c) Gross primary productivity (GPP) tends to peak earlier in the season for warmer sites, though the trend is weak. All r^2 values are significant at $p < 0.001$. Each point represents a site-year of data.

3.3.3 Uniqueness of tropical wetlands

Tropical wetlands typically do not experience the large swings in temperature and GPP that contribute to CH_4 flux seasonality in temperate and northern sites. Indeed, the relatively constant high temperatures and high GPP in tropical ecosystems may lead to the lower ratio between seasonal amplitude and peak CH_4 flux compared with temperate and northern sites (Fig. 8b). Tropical flux sites have historically been under-studied, leading to a lack of synthesized information about these ecosystems. FLUXNET-CH4 has five tropical wetland sites (latitude between 20° S and 20° N), and one tropical rice site, representing 13 site-years of data. These sites are especially insightful as they provide the first estimates of CH_4 fluxes from tropical, large seasonal floodplain systems.

We found a broad range of annual CH_4 fluxes across tropical sites in FLUXNET-CH4 Version 1.0. Annual CH_4 flux emissions from two Southeast Asian flooded peat forests were relatively low, 0.01 ± 0.1 and 9.5 ± 0.6 g C m^{-2} yr^{-1} for ID-PAG and MY-MLM, respectively, which is consistent with annual CH_4 fluxes measured at another peat forest in Indonesia (Deshmukh et al., 2020). In contrast, mean annual CH_4 flux for a seasonally flooded swamp in the Brazilian Pantanal region (BR-NPW) was over twice as high as MY-MLM, at 19.2 ± 2.5 g C m^{-2} yr^{-1}. Similarly high annual CH_4 fluxes were observed at the two Botswana swamp sites in the Okavango Delta (51.7 ± 10.6 and 47.3 ± 3.7 g C m^{-2} yr^{-1} for BW-GUM and BW-NXR, respectively), one of which is seasonally inundated and surrounded by grassland (BW-NXR) and the other is a permanently flooded lagoon covered in a floating papyrus mat (BW-GUM). The relatively low fluxes found at the two Southeast Asian peat forest sites indicate that these ecosystems may be smaller CH_4 sources than expected, given their location in the humid tropics. Even the higher-emitting tropical sites in Brazil and Botswana are still well within the range of annual CH_4 flux typical in cooler latitudes (Fig. 1).

In addition to having highly variable CH_4 flux magnitudes, the tropical sites differ from each other in their seasonality. CH_4 flux hit a minimum around July for two sites (BW-GUM, latitude 18.965 °S and MY-MLM, latitude 1.46 °N), while CH_4 flux increased through July and the subsequent months for the other Botswana site, BW-NXR (latitude 19.548 °S). Site ID-Pag (latitude 2.32 °S) had minimal seasonality, whereas the flooded forest site in Brazil (BR-NPW, latitude 16.49 °S) had near-zero fluxes from approximately July to January, and consistently high fluxes for the remainder of the year. The rice site PH-RiF (latitude 14.14 °N) had two annual CH_4 flux peaks, which is consistent with some other rice sites and likely reflects management practices. Baseline CH_4 flux values also differed, with the two Botswana sites having the highest off-season fluxes (29 and 133 nmol m^{-2} s^{-1} for BW-NXR and BW-GUM, respectively, estimated by Timesat), MY-MLM having an intermediate baseline CH_4 flux (16 nmol m^{-2} s^{-1}, estimated by Timesat), and the remainder of the sites having essentially zero flux at baseline. While more tropical wetland data will be needed to extract broad scale conclusions about these ecosystems, the six tropical sites in FLUXNET-CH4 provide an important starting point for synthesis studies and highlight tropical wetland CH_4 variability.

4.0 Data Availability

Half-hourly and daily aggregations are available for download at https://fluxnet.org/data/fluxnet-ch4-community-product/, along with a table containing site metadata compiled from Table B3. Variable descriptions and units are provided in Table B1, and at https://fluxnet.org/data/fluxnet-ch4-community-product/. Each site has a unique FLUXNET-CH4 DOI as listed in Table B3. All site data used in this analysis are available under the CC BY 4.0 (https://creativecommons.org/licenses/by/4.0/) copyright policy (2 additional sites in FLUXNET-CH4 are available under the more restrictive Tier 2 data policy, https://fluxnet.org/data/data-policy/; these sites are not used in our analysis). The individual site DOIs are provided below in Table 2. All seasonality parameters used in these analyses are available at https://doi.org/10.5281/zenodo.4672601.

Table 2: Site identification (SITE_ID), data DOI, and DOI reference for each FLUXNET-CH4 site.

SITE_ID	DOI	DOI_REFERENCE
AT-Neu	10.18140/FLX/1669365	Wohlfahrt et al., 2020.
BR-Npw	10.18140/FLX/1669368	Vourlitis et al., 2020.
BW-Gum	10.18140/FLX/1669370	Helfter, 2020a.
BW-Nxr	10.18140/FLX/1669518	Helfter, 2020b.
CA-SCB	10.18140/FLX/1669613	Sonnentag and Helbig, 2020a.
CA-SCC	10.18140/FLX/1669628	Sonnentag and Helbig, 2020b.
CH-Cha	10.18140/FLX/1669629	Hörtnagl et al., 2020a.
CH-Dav	10.18140/FLX/1669630	Hörtnagl et al., 2020b.
CH-Oe2	10.18140/FLX/1669631	Hörtnagl, et al., 2020c.
CN-Hgu	10.18140/FLX/1669632	Niu and Chen, 2020.
DE-Dgw	10.18140/FLX/1669633	Sachs et al, 2020a.
DE-Hte	10.18140/FLX/1669634	Koebsch and Jurasinski, 2020.
DE-SfN	10.18140/FLX/1669635	Klatt et al., 2020.
DE-Zrk	10.18140/FLX/1669636	Sachs et al., 2020b.
FI-Hyy	10.18140/FLX/1669637	Mammarella et al. 2020.
FI-Lom	10.18140/FLX/1669638	Aurela et al., 2020.
FI-Si2	10.18140/FLX/1669639	Vesala et al., 2020a.
FI-Sii	10.18140/FLX/1669640	Vesala et al., 2020b
FR-LGt	10.18140/FLX/1669641	Jacotot et al., 2020.
HK-MPM	10.18140/FLX/1669642	Lai and Liu, 2020.
ID-Pag	10.18140/FLX/1669643	Sakabe et al., 2020.
IT-BCi	10.18140/FLX/1669644	Magliulo et al., 2020.

IT-Cas	10.18140/FLX/1669645	Manca and Goded, 2020.
JP-BBY	10.18140/FLX/1669646	Ueyama et al., 2020.
JP-Mse	10.18140/FLX/1669647	Iwata, 2020a.
JP-SwL	10.18140/FLX/1669648	Iwata, 2020b.
KR-CRK	10.18140/FLX/1669649	Ryu et al., 2020.
MY-MLM	10.18140/FLX/1669650	~~Tang~~ Wong et al., 2020.
NL-Hor	10.18140/FLX/1669651	Dolman et al., 2020a.
NZ-Kop	10.18140/FLX/1669652	Campbell and Goodrich, 2020.
PH-RiF	10.18140/FLX/1669653	Alberto and Wassmann, 2020.
RU-Ch2	10.18140/FLX/1669654	Goeckede, 2020.
RU-Che	10.18140/FLX/1669655	Merbold et al., 2020.
RU-Cok	10.18140/FLX/1669656	Dolman et al., 2020b.
RU-Fy2	10.18140/FLX/1669657	Varlagin, 2020.
SE-Deg	10.18140/FLX/1669659	Nilsson and Peichl, 2020.
UK-LBT	10.18140/FLX/1670207	Helfter, 2020c.
US-A03	10.18140/FLX/1669661	Billesbach and Sullivan, 2020a.
US-A10	10.18140/FLX/1669662	Billesbach and Sullivan, 2020b.
US-Atq	10.18140/FLX/1669663	Zona and Oechel, 2020a.
US-Beo	10.18140/FLX/1669664	Zona and Oechel, 2020b.
US-Bes	10.18140/FLX/1669665	Zona and Oechel, 2020c.
US-Bi1	10.18140/FLX/1669666	Rey-Sanchez et al., 2020a.
US-Bi2	10.18140/FLX/1669667	Rey-Sanchez et al., 2020b.
US-BZB	10.18140/FLX/1669668	Euskirchen and Edgar, 2020a.
US-BZF	10.18140/FLX/1669669	Euskirchen and Edgar, 2020b.
US-BZS	10.18140/FLX/1669670	Euskirchen and Edgar, 2020c.

US-CRT	10.18140/FLX/1669671	Chen and Chu, 2020a.
US-DPW	10.18140/FLX/1669672	Hinkle and Bracho, 2020.
US-EDN	10.18140/FLX/1669673	Oikawa, 2020.
US-EML	10.18140/FLX/1669674	Schuur, 2020.
US-Ho1	10.18140/FLX/1669675	Richardson and Hollinger, 2020.
US-HRA	10.18140/FLX/1669676	Runkle et al., 2020.
US-HRC	10.18140/FLX/1669677	Reba et al., 2020.
US-ICs	10.18140/FLX/1669678	Euskirchen et al., 2020d.
US-Ivo	10.18140/FLX/1669679	Zona and Oechel, 2020d.
US-LA1	10.18140/FLX/1669680	Holm et al., 2020a.
US-LA2	10.18140/FLX/1669681	Holm et al., 2020b.
US-Los	10.18140/FLX/1669682	Desai and Thom, 2020a.
US-MAC	10.18140/FLX/1669683	Sparks, 2020.
US-MRM	10.18140/FLX/1669684	Schafer, 2020.
US-Myb	10.18140/FLX/1669685	Matthes et al., 2020.
US-NC4	10.18140/FLX/1669686	Noormets et al., 2020.
US-NGB	10.18140/FLX/1669687	Torn and Dengel, 2020a.
US-NGC	10.18140/FLX/1669688	Torn and Dengel, 2020b.
US-ORv	10.18140/FLX/1669689	Bohrer and Morin, 2020a.
US-OWC	10.18140/FLX/1669690	Bohrer et al., 2020b.
US-PFa	10.18140/FLX/1669691	Desai and Thom, 2020b.
US-Snd	10.18140/FLX/1669692	Detto et al., 2020.
US-Sne	10.18140/FLX/1669693	Short et al., 2020.
US-Srr	10.18140/FLX/1669694	Windham-Myers et al., 2020.
US-StJ	10.18140/FLX/1669695	Vazquez-Lule and Vargas, 2020.

US-Tw1	10.18140/FLX/1669696	Valach et al., 2020a.
US-Tw3	10.18140/FLX/1669697	Chamberlain et al., 2020.
US-Tw4	10.18140/FLX/1669698	Eichelmann et al., 2020.
US-Tw5	10.18140/FLX/1669699	Valach et al., 2020b.
US-Twt	10.18140/FLX/1669700	Knox et al., 2020.
US-Uaf	10.18140/FLX/1669701	Iwata et al., 2020c.
US-WPT	10.18140/FLX/1669702	Chen and Chu, 2020b.

5.0 Conclusions

The breadth and scope of CH_4 flux data in the FLUXNET-CH4 dataset make it possible to study the global patterns of CH_4 fluxes, particularly for global freshwater wetlands which release a substantial fraction of atmospheric CH_4. To help data users understand seasonal patterns within the dataset, we provide the first global estimates of CH_4 flux patterns and predictors in CH_4 seasonality using freshwater wetland data. In the seasonality analysis, we find that, on average, the seasonal increase in CH_4 emissions begins about three months earlier and lasts about four months longer at the warmest sites compared with the coolest sites. We also find that the beginning of the CH_4 emission season lags the beginning of seasonal soil warming by approximately one month, with almost no instances of CH_4 emissions increasing before temperature increases. Additionally, roughly half the sites have CH_4 emissions increasing prior to GPP increase; highlighting the importance of substrate versus temperature limitations on wetland CH_4 emissions. Furthermore, relative to warmer climates, wetland CH_4 emissions in cooler climates increase faster in the warming season and decrease slower in the cooling season. This phenomenon has previously been noted on a regional scale and we show that it persists at the global scale. Constraining the seasonality of CH_4 fluxes on a global scale can help improve the accuracy of global wetland models.

FLUXNET-CH4 is an important new resource for the research community, but critical data gaps and opportunities remain. The current FLUXNET-CH4 dataset is biased towards sites in boreal and temperate regions, which influence the relationships presented in our analyses. Tropical ecosystems are estimated to account for 64% of potential natural CH_4 emissions (<30° N, Saunois et al., 2020) but only account for 13% of the FLUXNET-CH4 sites in the dataset. Unsurprisingly, tropical sites in our network do not represent the range of bioclimatic wetland conditions present in the tropics. Therefore, while maintaining flux towers in tropical ecosystems is challenging, it is necessary to further constrain the global CH_4 cycle. Coastal wetlands are also poorly represented in FLUXNET-CH4 even though there is evidence of substantial CH_4 emissions from these ecosystems, so better representation across salinity gradients is warranted. Lastly, the average time series for FLUXNET-CH4 Version 1.0 is relatively short, only 3.7 site-years on average compared with 7.2 for CO_2 sites in FLUXNET (Pastorello et al., 2020). Adding additional site-years of data from existing sites, as a complement to adding new sites, will increase the community's ability to explain interannual variability in CH_4 emission and seasonality. Nevertheless, FLUXNET-CH4 is an important and unprecedented resource with which to diagnose and understand drivers of the global CH_4 cycle.

Author contribution

Kyle B. Delwiche oversaw the data release, performed the seasonality analysis, gathered metadata, and prepared the manuscript with contributions from all co-authors. Sara Helen Knox gathered and standardized the data, and gap-filled the CH_4 flux data. Avni Malhotra prepared the manuscript and gathered metadata. Etienne Fluet-Chouinard did the representativeness analysis and prepared the manuscript. Gavin McNicol gathered data and prepared the manuscript. Robert B. Jackson oversaw the data collection, processing, analysis, and release. Danielle Christianson and You-Wei Cheah oversaw the FLUXNET-CH4 dataset release on fluxnet.org. Dario Papale, Eleonora Canfora, and Carlo Trotta did the data collection, curation, and pre-processing for all of the sites outside North and South America. Remaining co-authors contributed eddy-covariance data to FLUXNET-CH4 dataset and/or participated in editing the manuscript.

Competing interests

The authors declare that they have no conflict of interest.

Acknowledgements

We acknowledge primary support from the Gordon and Betty Moore Foundation (Grant GBMF5439, "Advancing Understanding of the Global Methane Cycle"; Stanford University) and from the John Wesley Powell Center for Analysis and Synthesis of the U.S. Geological Survey ("Wetland FLUXNET Synthesis for Methane" working group). Benjamin R. K. Runkle was supported by the U.S. National Science Foundation CBET CAREER Award 1752083. Ankur R. Desai acknowledges support of the DOE AmeriFlux Network Management Project. Masahito Ueyama was supported by ArCS II (JPMXD1420318865) and JSPS KAKENHI (20K21849). Dario Papale and Nina Buchmann acknowledge the support of the RINGO (GA 730944) H2020 EU project. Nina Buchmann and Kathrin Fuchs acknowledge the SNF project M4P (40FA40_154245/1) and InnoFarm (407340_172433). Nina Buchmann acknowledges support from the SNF for ICOS-CH Phases 1 and 2 (20FI21_148992, 20FI20_173691). Carlo Trotta acknowledges the support of the E-SHAPE (GA 820852) H2020 EU project. William J. Riley was supported by the US Department of Energy, BER, RGCM, RUBISCO project under contract no. DEAC02-05CH11231. Jessica Turner acknowledges support from NSF GRFP (DGE-1747503) and NTL LTER (DEB-1440297). Minseok Kang was supported by the National Research Foundation of Korea (NRF-2018 R1C1B6002917). Carole Helfter acknowledges the support of the UK Natural Environment Research Council (the Global Methane Budget project, grant number NE/N015746/1). Rodrigo Vargas acknowledges support from the National Science Foundation (1652594). Dennis Baldocchi acknowledges the California Department of Water Resources for a funding contract from the California Department of Fish and Wildlife and the United States Department of Agriculture (NIFA grant #2011-67003-30371), as well as the U.S. Department of Energy's Office of Science (AmeriFlux contract #7079856) for funding the AmeriFlux core sites. US-A03 and US-A10 are operated by the Atmospheric Radiation Measurement (ARM) user facility, a U.S. Department of Energy Office of Science user facility managed by the Biological and Environmental Research Program (doi:10.5439/1025039, doi:10.5439/1025274, doi:10.5439/1095578). Work at ANL was supported by the U.S. Department of Energy, Office of Science, Office of Biological and Environmental Research, under contract DE-AC02-06CH11357. Any use of trade, firm, or product names is for descriptive purposes only and does not imply endorsement by the U.S. Government. The CH-Dav, DE-SfN, FI-Hyy, FI-Lom, FI-Sii, FR-LGt, IT-BCi, SE-Deg and SE-Sto sites are part of the ICOS European Research Infrastructure. Oliver Sonnentag acknowledges funding by the Canada Research Chairs, Canada Foundation for Innovation Leaders Opportunity Fund, and Natural Sciences and Engineering Research Council Discovery Grant Programs for work at CA-SCC and CA-SCB. Benjamin Poulter acknowledges support from the NASA Carbon Cycle and Ecosystems Program. Derrick Lai acknowledges the support of the Research Grants Council of the Hong Kong Special Administrative Region, China (Project No. CUHK 458913).We thank Nathaniel Goenawan for his help with the representativeness analysis.

References

Abdalla, M., Hastings, A., Truu, J., Espenberg, M., Mander, Ü, Smith, P. Emissions of methane from northern peatlands: a review of management impacts and implications for future management options. Ecol. Evol., 6, 7080-7102. https://doi.org/10.1002/ece3.2469.

Alberto, M. C. R., Wassmann, R., Gummert, M., Buresh, R. J., Quilty, J. R., Correa, T. Q., Centeno, C. A. R., & Oca, G. M. Straw incorporated after mechanized harvesting of irrigated rice affects net emissions of CH4 and CO2 based on eddy covariance measurements. Field Crop. Res., 184, 162–175. https://doi.org/10.1016/j.fcr.2015.10.004. 2015.

Alberto, M., & Wassmann, R. FLUXNET-CH4 PH-RiF Philippines Rice Institute flooded. Philippines. https://doi:10.18140/FLX/1669653. 2020.

Anderson, D. E., Verma, S. B., & Rosenberg, N. J. Eddy correlation measurements of CO2, latent heat, and sensible heat fluxes over a crop surface. Bound. Lay. Meteorol., 29(3), 263–272. https://doi.org/10.1007/bf00119792. 1984.

Anderson, F. E., Bergamaschi, B., Sturtevant, C., Knox, S., Hastings, L., Windham-Myers, L., Detto, M., Hestir, E. L., Drexler, J., Miller, R. L., Matthes, J. H., Verfaillie, J., Baldocchi, D., Snyder, R. L., & Fujii R. Variation of energy and carbon fluxes from a restored temperate freshwater wetland and implications for carbon market verification protocols. J. of Geophys. Res. – Biogeo., 121(3), 777–795. https://doi.org/10.1002/2015JG003083. 2016.

Angle, J. C., Morin, T. H., Solden, L. M., Narrowe, A. B., Smith, G. J., Borton, M. A., Rey-Sanchez, C., Daly, R. A., Mirfenderesgi, G., Hoyt, D. W., Riley, W. J., Miller, C. S., Bohrer, G., & Wrighton, K. C. Methanogenesis in oxygenated soils is a substantial fraction of wetland methane emissions. Nat. Comm., 8(1), 1567. https://doi.org/10.1038/s41467-017-01753-4. 2017.

Aurela, M., Lohila, A., J.-P., Hatakka, J., Rainne, J., Mäkelä, T., & Lauria, T. FLUXNET-CH4 FI-Lom Lompolojankka. Finland. https://doi:10.18140/FLX/1669638. 2020.

Bartlett, K. B., Bartlett, D. S., Harriss, R. C., & Sebacher, D. I. Methane emissions along a salt marsh salinity gradient. Biogeochemistry, 4(3), 183–202. https://doi.org/10.1007/bf02187365. 1987.

Bastviken, D., Tranvik, L. J., Downing, J. A., Crill, P. M., & Enrich-Prast, A. Freshwater methane emissions offset the continental carbon sink. Science, 331(6013), 50. https://doi.org/10.1126/science.1196808. 2011.

Billesbach, D., & Sullivan, R. FLUXNET-CH4 US-A03 ARM-AMF3-Oliktok. United States. https:// doi:10.18140/FLX/1669661. 2020a.

Billesbach, D., & Sullivan, R. FLUXNET-CH4 US-A10 ARM-NSA-Barrow. United States. https://doi:10.18140/FLX/1669662. 2020b.

Bloom, A. A., Bowman, K. W., Lee, M., Turner, A. J., Schroeder, R., Worden, J. R., Weidner, R., McDonald, K. C., & Jacob, D. J. A global wetland methane emissions and uncertainty dataset for atmospheric chemical transport models (WetCHARTs version 1.0). Geosci. Model Dev., 10, 2141-2156. https://doi.org/10.5194/gmd-10-2141-2017. 2017.

Bridgham, S. D., Cadillo-Quiroz, H., Keller, J. K., & Zhuang, Q. Methane emissions from wetlands: biogeochemical, microbial, and modeling perspectives from local to global scales. Glob. Change Biol., 19(5), 1325–1346. https://doi.org/10.1111/gcb.12131. 2013.

Bohrer, G., & Morin, T. H. FLUXNET-CH4 US-ORv Olentangy River Wetland Research Park. United States. https://doi:10.18140/FLX/1669689. 2020a.

Bohrer, G., Kerns, J., Morin, T. H., Rey-Sanchez, A. C., Villa, J., & Ju, Y. FLUXNET-CH4 US-OWC Old Woman Creek. United States. https://doi:10.18140/FLX/1669690. 2020b.

Campbell, D., & Goodrich, J. FLUXNET-CH4 NZ-Kop Kopuatai. New Zealand. https://doi:10.18140/FLX/1669652. 2020.

Castro-Morales, K., Kleinen, T., Kaiser, S., Zaehle, S., Kittler, F., Kwon, M. J., Beer, C., & Göckede, M. Year-round simulated methane emissions from a permafrost ecosystem in Northeast Siberia. Biogeosciences, 15(9), 2691–2722. https://doi.org/10.5194/bg-15-2691-2018. 2018.

Chadburn, S. E., Aalto, T., Aurela, M., Baldocchi, D., Biasi, C., Boike, J., Burke, E. J., Comyn-Platt, E., Dolman, A. J., Duran-Rojas, & Others. Modeled microbial dynamics explain the apparent temperature sensitivity of wetland methane emissions. Global Biogeochemical Cycles, 34(11). https://doi.org/10.1029/2020gb006678. 2020.

Chamberlain, S. D., Oikawa, P., Sturtevant, C., Szutu, D., Verfaillie, J., & Baldocchi, D. FLUXNET-CH4 US-Tw3 Twitchell Alfalfa. United States. https://doi:10.18140/FLX/1669697. 2020.

Chambers, L. G., Ramesh Reddy, K., & Osborne, T. Z. Short-Term Response of Carbon Cycling to Salinity Pulses in a Freshwater Wetland. Soil Sci. Soc. Am. J., 75(5), 2000–2007. https://doi.org/10.2136/sssaj2011.0026. 2011.

Chang, K. Y., W. J. Riley, S. H. Knox, R. B. Jackson, G. McNicol, B. Poulter, M. Aurela, D. Baldocchi, S. Bansal, G. Bohrer, D. I. Campbell, A. Cescatti, H. Chu, K. B. Delwiche, A. Desai, E. Euskirchen, T. Friborg, M. Goeckede, G. Holm, M. Kang, T. Keenan, K. W. Krauss, A. Lohila, I. Mammarella, A. Miyata, M. B. Nilsson, A. Noormets, D. Papale, B. R. K. Runkle, Y. Ryu, T. Sachs, K. V. R. Schäfer, H. P. Schmid, N. Shurpali, O. Sonnentag, A. C. I. Tang, M. S. Torn, C. Trotta, M. Ueyama, R. Vargas, T. Vesala, L. Windham-Myers, Z. Zhang, & D. Zona. Global wetland methane emissions have hysteretic responses to seasonal temperature. Nature Communications, 12. 2266. ~~[In press]~~. https://doi.org/10.1038/s41467-021-22452-1. 2021

Chanton, J. P., Glaser, P. H., Chasar, L. S., Burdige, D. J., Hines, M. E., Siegel, D. I., Tremblay, L. B., & Cooper, W. T. Radiocarbon evidence for the importance of surface vegetation on fermentation and methanogenesis in contrasting types of boreal peatlands. Global Biogeochem. Cy., 22(4). https://doi.org/10.1029/2008gb003274. 2008.

Chen, J., & Chu, H. FLUXNET-CH4 US-CRT Curtice Walter-Berger cropland. United States. https://doi:10.18140/FLX/1669671. 2020a.

Chen, J., & Chu, H. FLUXNET-CH4 US-WPT Winous Point North Marsh. United States. https://doi:10.18140/FLX/1669702. 2020b.

Chu, H., Chen, J., Gottgens, J. F., Ouyang, Z., John, R., Czajkowski, K., & Becker, R. Net ecosystem methane and carbon dioxide exchanges in a Lake Erie coastal marsh and a nearby cropland. J. Geophys. Res.: Biogeo., 119(5), 722–740. https://doi.org/10.1002/2013JG002520. 2014.

Chu, H., Baldocchi, D. D., John, R., Wolf, S., & Reichstein, M. Fluxes all of the time? A primer on the temporal representativeness of FLUXNET. Journal of Geophysical Research: Biogeosciences, 122(2), 289–307. https://doi.org/10.1002/2016JG003576. 2017.

Chu, H., Luo, X., Ouyang, Z., Chan, W. S., Dengel, S., Biraud, S. C., Torn, M. S., Metzger, S., Kumar, J., Arain, M. A., & Others. Representativeness of Eddy-Covariance flux footprints for areas surrounding AmeriFlux sites. Agricultural and Forest Meteorology, 301-302, 108350. https://doi.org/10.1016/j.agrformet.2021.108350. 2021.

Dalcin Martins, P., Hoyt, D. W., Bansal, S., Mills, C. T., Tfaily, M., Tangen, B. A., Finocchiaro, R. G., Johnston, M. D., McAdams, B. C., Solensky, M. J., Smith, G. J., Chin, Y.-P., & Wilkins, M. J. Abundant carbon substrates drive extremely high sulfate reduction rates and methane fluxes in Prairie Pothole Wetlands. Global Change Biology, 23(8), 3107–3120. https://doi.org/10.1111/gcb.13633. 2017.

Dean, J. F., Middelburg, J. J., Röckmann, T., Aerts, R., Blauw, L. G., Egger, M., Jetten, M. S. M., de Jong, A. E. E., Meisel, O. H., Rasigraf, O., Slomp, C. P., in't Zandt, M. H., & Dolman, A. J. Methane Feedbacks to the Global Climate System in a Warmer World. Rev. Geophys., 56(1), 207–250. https://doi.org/10.1002/2017rg000559. 2018.

Deemer, B. R., Harrison, J. A., Li, S., Beaulieu, J. J., DelSontro, T., Barros, N., Bezerra-Neto, J. F., Powers, S. M., Dos Santos, M. A., & Vonk, J. A. Greenhouse Gas Emissions from Reservoir Water Surfaces: A New Global Synthesis. Bioscience, 66(11), 949–964. https://doi.org/10.1093/biosci/biw117. 2016.

Dengel, S., Zona, D., Sachs, T., Aurela, M., Jammet, M., Parmentier, F.-J. W., Oechel, W., & Vesala, T. Testing the applicability of neural networks as a gap-filling method using CH4 flux data from high latitude wetlands. Biogeosciences, 10, 8185–8200. https://doi.org/10.5194/bg-10-8185-2013. 2013.

Deshmukh, C. S., Julius, D., Evans, C. D., Nardi, Susanto, A. P., Page, S. E., Gauci, V., Laurén, A., Sabiham, S., Agus, F., Asyhari, A., Kurnianto, S., Suardiwerianto, Y., & Desai, A. R. Impact of forest plantation on methane emissions from tropical peatland. Glob. Change Biol., 26, 2477-2495. https://doi.org/10.1111/gcb.15019. 2020.

Desai, A. R., & Thom, J. FLUXNET-CH4 US-Los Lost Creek. United States. https://doi:10.18140/FLX/1669682. 2020a.

Desai, A. R., & Thom, J. FLUXNET-CH4 US-PFa Park Falls/WLEF. United States. https://doi:10.18140/FLX/1669691. 2020b.

Desjardins, R. L. A technique to measure CO2 exchange under field conditions. Int. J. Biometeorol., 18(1), 76–83. https://doi.org/10.1007/bf01450667. 1974.

Detto, M., Sturtevant, C., Oikawa, P., Verfaillie, J., & Baldocchi, D. FLUXNET-CH4 US-Snd Sherman Island. United States. https://doi:10.18140/FLX/1669692. 2020.

Dise, N. Winter fluxes of methane from Minnesota peatlands. Biogeochemistry, 17(2). https://doi.org/10.1007/bf00002641. 1992.

Dolman, H., Hendriks, D., Parmentier, F.-J., Marchesini, L. B., Dean, J., & van Huissteden, K. FLUXNET-CH4 NL-Hor Horstermeer. Netherlands. https://doi:10.18140/FLX/1669651. 2020a.

Dolman, H., van der Molen, H., Parmentier, F.-J., Marchesini, L. B., Dean, J., van Huissteden, K., & Maximov, T. FLUXNET-CH4 RU-Cok Chokurdakh. Russian Federation. https://doi:10.18140/FLX/1669656. 2020b.

Eichelmann, E., Knox, S., Rey Sanchez, C., Valach, A., Sturtevant, C., Szutu, D., Verfaillie, J., & Baldocchi, D. FLUXNET-CH4 US-Tw4 Twitchell East End Wetland. United States. https://doi:10.18140/FLX/1669698. 2020.

Eklundh, L., & Jönsson, P. TIMESAT: A Software Package for Time-Series Processing and Assessment of Vegetation Dynamics. Remote Sensing Time Series (pp. 141–158). https://doi.org/10.1007/978-3-319-15967-6_7. 2015.

Etheridge, D. M., Steele, L. P., Francey, R. J., & Langenfelds, R. L. Atmospheric methane between 1000 A.D. and present: Evidence of anthropogenic emissions and climatic variability. J. Geophys. Res. – Atmos., 103(D13), 15979–15993. https://doi.org/10.1029/98jd00923. 1998.

Etminan, M., Myhre, G., Highwood, E. J., & Shine, K. P. Radiative forcing of carbon dioxide, methane, and nitrous oxide: A significant revision of the methane radiative forcing. Geophys. Res. Lett., 43(24), 12,614–12,623. https://doi.org/10.1002/2016gl071930. 2016.

Euskirchen, E., & Edgar, C. FLUXNET-CH4 US-BZB Bonanza Creek Thermokarst Bog. United States. https://doi:10.18140/FLX/1669668. 2020a.

Euskirchen, E., & Edgar, C. FLUXNET-CH4 US-BZF Bonanza Creek Rich Fen. United States. https://doi:10.18140/FLX/1669669. 2020b.

Euskirchen, E., & Edgar, C. FLUXNET-CH4 US-BZS Bonanza Creek Black Spruce. United States. https://doi:10.18140/FLX/1669670. 2020c.

Euskirchen, E., Bret-Harte, M., & Edgar, C Marion Bret-Harte. FLUXNET-CH4 US-ICs Imnavait Creek Watershed Wet Sedge Tundra. United States. https://doi:10.18140/FLX/1669678. 2020d.

Gallant, A. The Challenges of Remote Monitoring of Wetlands. Remote Sensing, 7(8), 10938–10950. https://doi.org/10.3390/rs70810938. 2015.

Göeckede, M., Kittler, F., & Schaller, C. Quantifying the impact of emission outbursts and non-stationary flow on eddy covariance CH4 flux measurements using wavelet techniques. Biogeosciences, 16(16), 3113–3131. https://doi.org/10.5194/bg-16-3113-2019. 2019.

Goeckede, M. FLUXNET-CH4 RU-Ch2 Chersky reference. Russian Federation. https://doi:10.18140/FLX/1669654. 2020.

Gu, L., Post, W. M., Baldocchi, D. D., Andrew Black, T., Suyker, A. E., Verma, S. B., Vesala, T., & Wofsy, S. C. Characterizing the Seasonal Dynamics of Plant Community Photosynthesis Across a Range of Vegetation Types. In: Noormets A. (eds) Phenology of Ecosystem Processes. Springer, New York, NY. pp. 35–58. https://doi.org/10.1007/978-1-4419-0026-5_2. 2009.

Hargreaves, K. J., Fowler, D., Pitcairn, C. E. R., & Aurela, M. Annual methane emission from Finnish mires estimated from eddy covariance campaign measurements. Theor. Appl. Climatol., 70, 203–213. https://doi.org/10.1007/s007040170015. 2001.

Hargrove, W. W., Hoffman, F. M., & Law, B. E. New analysis reveals representativeness of the AmeriFlux network. Eos, Transactions American Geophysical Union, 84(48), 529. https://doi.org/10.1029/2003EO480001. 2003.

Hatala, J. A., Detto, M., & Baldocchi, D. D. Gross ecosystem photosynthesis causes a diurnal pattern in methane emission from rice. Geophys. Res. Lett., 39(6). https://doi.org/10.1029/2012gl051303. 2012.

Helbig, M., Quinton, W. L., & Sonnentag, O. Warmer spring conditions increase annual methane emissions from a boreal peat landscape with sporadic permafrost. Environ. Res. Lett., 12(11), 115009. https://doi.org/10.1088/1748-9326/aa8c85. 2017.

Helfter, C., Tremper, A. H., Halios, C. H., Kotthaus, S., Bjorkegren, A., Grimmond, C. S. B., Barlow, J. F., & Nemitz, E. Spatial and temporal variability of urban fluxes of methane, carbon monoxide and carbon dioxide above London, UK. Atmos. Chem. Phys. 16, 10543-10557. https://doi.org/10.5194/acp-2016-216-ac1. 2016.

Helfter, C. FLUXNET-CH4 BW-Gum Guma. Botswana. https://doi:10.18140/FLX/1669370. 2020a.

Helfter, C. FLUXNET-CH4 BW-Nxr Nxaraga. Botswana. https://doi:10.18140/FLX/1669518. 2020b.

Helfter, C. FLUXNET-CH4 UK-LBT London_BT. United Kingdom. https://doi:10.18140/FLX/1670207. 2020c.

Hinkle, C. R., & Bracho, R. FLUXNET-CH4 US-DPW Disney Wilderness Preserve Wetland. United States. https://doi:10.18140/FLX/1669672. 2020.

Hoffman, F. M., Kumar, J., Mills, R. T., & Hargrove, W. W. Representativeness-based sampling network design for the State of Alaska. Landscape Ecol., 28(8), 1567–1586. https://doi.org/10.1007/s10980-013-9902-0. 2013.

Hollinger, D. Y., and A. D. Richardson. Uncertainty in Eddy Covariance Measurements and Its Application to Physiological Models. Tree Physiology 25 (7): 873–85. https://doi.org/10.1093/treephys/25.7.873. 2005.

Holm, G. O., Perez, B. C., McWhorter, D. E., Krauss, K. W., Raynie, R. C., & Killebrew, C. J. FLUXNET-CH4 US-LA1 Pointe-aux-Chenes Brackish Marsh. United States. https://doi:10.18140/FLX/1669680. 2020a.

Holm, G. O., Perez, B. C., McWhorter, D. E., Krauss, K. W., Raynie, R. C., & Killebrew, C. J. FLUXNET-CH4 US-LA2 Salvador WMA Freshwater Marsh. United States. https://doi:10.18140/FLX/1669681. 2020b.

Hörtnagl, L., Feigenwinter, I. Fuchs, K., Merbold, L., Buchmann, N., Eugster, W., Zeeman, M., Pluess, P., Käslin, F., Meier, P., Koller, P., & Baur, T. FLUXNET-CH4 CH-Cha Chamau. Switzerland. https://doi:10.18140/FLX/1669629. 2020a.

Hörtnagl, Lukas, Werner Eugster, Lutz Merbold, Nina Buchmann, Mana Gharun, Sophia Etzold, Rudolf Haesler, Matthias Haeni, Philip Meier, Florian Käslin, Thomas Baur, & Peter Pluess. FLUXNET-CH4 CH-Dav Davos. Switzerland. https://doi:10.18140/FLX/1669630. 2020b.

Hörtnagl, Lukas, Regine Maier, Werner Eugster, Nina Buchmann, Carmen Emmel, Patrick Koller, Thomas Baur, Peter Pluess, Florian Käslin, & Philip Meier. FLUXNET-CH4 CH-Oe2 Oensingen crop. Switzerland. https://doi:10.18140/FLX/1669631. 2020c.

Hwang, Y., Ryu, Y., Huang, Y., Kim, J., Iwata, H., & Kang, M. Comprehensive assessments of carbon dynamics in an intermittently-irrigated rice paddy. Agr. Forest Met., 285–286, 107933. https://doi.org/10.1016/j.agrformet.2020.107933. 2020.

Iwata, H., Mano, M., Ono, K., Tokida, T., Kawazoe, T., Kosugi, Y., Sakabe, A., Takahashi, K., & Miyata, A. Exploring sub-daily to seasonal variations in methane exchange in a single-crop rice paddy in central Japan. Atmos. Environ., 179, 156–165. https://doi.org/10.1016/j.atmosenv.2018.02.015. 2018.

Iwata, Hiroki. FLUXNET-CH4 JP-Mse Mase rice paddy field. Japan. https://doi:10.18140/FLX/1669647. 2020a.

Iwata, Hiroki. FLUXNET-CH4 JP-SwL Suwa Lake. Japan. https://doi:10.18140/FLX/1669648. 2020b.

Iwata, Hiroki, Masahito Ueyama, & Yoshinobu Harazono. FLUXNET-CH4 US-Uaf University of Alaska, Fairbanks. United States. https://doi:10.18140/FLX/1669701. 2020c.

Jacotot, Adrien, Sébastien Gogo, & Fatima Laggoun-Défarge. FLUXNET-CH4 FR-LGt La Guette. France. https://doi:10.18140/FLX/1669641. 2020.

Jung, M., Reichstein, M., & Bondeau, A. Towards global empirical upscaling of FLUXNET eddy covariance observations: validation of a model tree ensemble approach using a biosphere model. Biogeosciences, 6(10), 2001–2013. https://doi.org/10.5194/bg-6-2001-2009. 2009.

Jung, M., Schwalm, C., Migliavacca, M., Walther, S., Camps-Valls, G., Koirala, S., Anthoni, P., Besnard, S., Bodesheim, P., Carvalhais, N., Chevallier, F., Gans, F., Goll, D. S., Haverd, V., Kohler, P., Ichii, K., Jain, A. K., Liu, J., Lombardozzi, D., Nabel, J. E. M. S., Nelson, J. A., O'Sullivan, M., Pallandt, M., Papale, D., Peters, W., Pongrats, J., Rodenbeck, C., Sitch, S. Tramontana, G., Walker, A., Weber, U., & Reichstein, M. Scaling carbon fluxes from eddy covariance sites to globe: synthesis and evaluation of the FLUXCOM approach. Biogeosciences, 17(5), 1343–1365. https://doi.org/10.5194/bg-17-1343-2020. 2020.

Kim, Y., Johnson, M. S., Knox, S. H., Andrew Black, T., Dalmagro, H. J., Kang, M., Kim, J., & Baldocchi, D. Gap-filling approaches for eddy covariance methane fluxes: A comparison of three machine learning algorithms and a traditional method with principal component analysis. Glob. Change Biol., 26(3), 1499–1518. https://doi.org/10.1111/gcb.14845. 2020.

Kittler, F., Heimann, M., Kolle, O., Zimov, N., Zimov, S., & Göckede, M. Long-Term Drainage Reduces CO_2 Uptake and CH_4 Emissions in a Siberian Permafrost Ecosystem: Drainage impact on Arctic carbon cycle. Global Biogeochem. Cy., 31(12), 1704–1717. https://doi.org/10.1002/2017GB005774. 2017.

Klatt, Janina, Hans Peter Schmid, Matthias Mauder, & Rainer Steinbrecher. FLUXNET-CH4 DE-SfN Schechenfilz Nord. Germany. https://doi:10.18140/FLX/1669635. 2020.

Knox, S. H., Sturtevant, C., Matthes, J. H., Koteen, L., Verfaillie, J., & Baldocchi, D. Agricultural peatland restoration: effects of land-use change on greenhouse gas (CO_2 and CH_4) fluxes in the Sacramento-San Joaquin Delta. Glob. Change Biol., 21(2), 750–765. https://doi.org/10.1111/gcb.12745. 2015.

Knox, S. H., Matthes, J. H., Sturtevant, C., Oikawa, P. Y., Verfaillie, J., & Baldocchi, D. Biophysical controls on interannual variability in ecosystem-scale $CO_2$and CH_4exchange in a California rice paddy. J. Geophys. Res.-Biogeo., 121(3), 978–1001. https://doi.org/10.1002/2015jg003247. 2016.

Knox, S. H., Jackson, R. B., Poulter, B., McNicol, G., Fluet-Chouinard, E., Zhang, Z., Hugelius, G., Bousquet, P., Canadell, J. G., Saunois, M., Papale, D., Chu, H., Keenan, T. F., Baldocchi, D., Torn, M. S., Mammarella, I., Trotta, C., Aurela, M., Bohrer, G., Campbell, D.I., Cescatti, A., Chamberlain, S., Chen, J., Chen, W., Dengel, S., Desai, A.R., Euskirchen, E., Friborg, T., Gasbarra, D., Goded, I., Goeckede, M., Heimann, M., Helbig, M., Hirano, T., Hollinger, D.Y., Iwata, H., & Others. FLUXNET-CH4 Synthesis Activity: Objectives, Observations, and Future Directions. B. Am. Meterol. Soc., 100(12), 2607–2632. https://doi.org/10.1175/bams-d-18-0268.1. 2019.

Knox, Sara, Jaclyn Hatala Matthes, Joseph Verfaillie, & Dennis Baldocchi. FLUXNET-CH4 US-Twt Twitchell Island. United States. https://doi:10.18140/FLX/1669700. 2020.

Koebsch, F., Jurasinski, G., Koch, M., Hofmann, J., & Glatzel, S. Controls for multi-scale temporal variation in ecosystem methane exchange during the growing season of a permanently inundated fen. Agr. Forest Meteorol., 204, 94–105. https://doi.org/10.1016/j.agrformet.2015.02.002. 2015.

Koebsch, F., Winkel, M., Liebner, S., Liu, B., Westphal, J., Schmiedinger, I., Spitzy, A., Gehre, M., Jurasinski, G., Köhler, S., & Others. Sulfate deprivation triggers high methane production in a disturbed and rewetted coastal peatland. Biogeosciences, 16, 1937–1953. https://doi.org/10.5194/bg-16-1937-2019. 2019.

Koebsch, Franziska, & Gerald Jurasinski. FLUXNET-CH4 DE-Hte Huetelmoor. Germany. https://doi:10.18140/FLX/1669634. 2020.

Kuznetsova A., Brockhoff P.B., & Christensen R. H. B. “lmerTest Package: Tests in Linear Mixed Effects Models.” Journal of Statistical Software, 82(13), 1-26. https://doi.org/10.18637/jss.v082.i13. 2017.

Kwon, M. J., Beulig, F., Ilie, I., Wildner, M., Küsel, K., Merbold, L., Mahecha, M. D., Zimov, N., Zimov, S. A., Heimann, M., Schuur, E. A. G., Kostka, J. E., Kolle, O., Hilke, I., & Göckede, M. Plants, microorganisms, and soil temperatures contribute to a decrease in methane fluxes on a drained Arctic floodplain. Global Change Biology, 23(6), 2396–2412. https://doi.org/10.1111/gcb.13558. 2017.

Lai, D. Y. F. Methane Dynamics in Northern Peatlands: A Review. Pedosphere, 19(4), 409–421. https://doi.org/10.1016/s1002-0160(09)00003-4. 2009.

Lai, D. Y. F., Roulet, N. T., & Moore, T. R. The spatial and temporal relationships between CO2 and CH4 exchange in a temperate ombrotrophic bog. Atmos. Environ, 89, 249–259. https://doi.org/10.1016/j.atmosenv.2014.02.034. 2014.

Lai, Derrick Y.F., & Jiangong Liu. FLUXNET-CH4 HK-MPM Mai Po Mangrove. Hong Kong. https://doi:10.18140/FLX/1669642. 2020.

Lasslop, G., Reichstein, M., Papale, D., Richardson, A. D., Arneth, A., Barr, A., Stoy, P., & Wohlfahrt, G. Separation of net ecosystem exchange into assimilation and respiration using a light response curve approach: critical issues and global evaluation. Glob. Change Biol., 16(1), 187–208. https://doi.org/10.1111/j.1365-2486.2009.02041.x. 2010.

Liu, J., Zhou, Y., Valach, A., Shortt, R., Kasak, K., Rey-Sanchez, C., Hemes, K. S., Baldocchi, D., & Lai, D. Y. F. Methane emissions reduce the radiative cooling effect of a subtropical estuarine mangrove wetland by half. Glob. Change Biol., 26(9), 4998–5016. https://doi.org/10.1111/gcb.15247. 2020.

Madsen, K., Nielsen, H. B., & Tingleff, O. Methods for non-linear least squares problems. Informatics and Mathematical Modelling, Technical Univeristy of Denmark. 2nd Edition. 2004.

Magliulo, Vincenzo, Paul Di Tommasi, Daniela Famulari, Daniele Gasbarra, Luca Vitale, Antonio Manco, Ferdinando di Matteo, Andrea Esposito, & Maurizio Tosca. FLUXNET-CH4 IT-BCi Borgo Cioffi. Italy. https://doi:10.18140/FLX/1669644. 2020.

Mahecha, M. D., Gans, F., Sippel, S., Donges, J. F., Kaminski, T., Metzger, S., Migliavacca, M., Papale, D., Rammig, A., & Zscheischler, J. Detecting impacts of extreme events with ecological in situ monitoring networks. Biogeosciences, 14(18), 4255–4277. https://doi.org/10.5194/bg-14-4255-2017. 2017.

Malhotra, A., & Roulet, N. T. Environmental correlates of peatland carbon fluxes in a thawing landscape: do transitional thaw stages matter? Biogeosciences, 12(10), 3119–3130. https://doi.org/10.5194/bg-12-3119-2015. 2015.

Mammarella, Ivan, Timo Vesala, Petri Keronen, Pasi Kolari, Samuli Launiainen, Jukka Pumpanen, Üllar Rannik, Erkki Siivola, Janne Levula, & Toivo Pohja. FLUXNET-CH4 FI-Hyy Hyytiala. Finland. https://doi:10.18140/FLX/1669637. 2020.

Manca, Giovanni, & Ignacio Goded. FLUXNET-CH4 IT-Cas Castellaro. Italy. https://doi:10.18140/FLX/1669645. 2020.

Mastepanov, M., Sigsgaard, C., Tagesson, T., Ström, L., Tamstorf, M. P., Lund, M., & Christensen, T. R. Revisiting factors controlling methane emissions from high-Arctic tundra. Biogeosciences, 10(7), 5139–5158. https://doi.org/10.5194/bg-10-5139-2013. 2013.

Matthes, Jaclyn Hatala, Cove Sturtevant, Patty Oikawa, Samuel D Chamberlain, Daphne Szutu, Ariane Arias Ortiz, Joseph Verfaillie, & Dennis Baldocchi. FLUXNET-CH4 US-Myb Mayberry Wetland. United States. https://doi:10.18140/FLX/1669685. 2020.

Matthews, E., Johnson, M. S., Genovese, V., Du, J., & Bastviken, D. Methane emission from high latitude lakes: methane-centric lake classification and satellite-driven annual cycle of emissions. Sci. Rep.- UK, 10(1), 12465. https://doi.org/10.1038/s41598-020-68246-1. 2020.

Megonigal, J. P., Whalen, S. C., Tissue, D. T., Bovard, B. D., Allen, A. S., & Albert, D. B. A Plant-Soil-Atmosphere Microcosm for Tracing Radiocarbon from Photosynthesis through Methanogenesis. Soil Sci. Soc. Am. J. 63(3), 665–671. https://doi.org/10.2136/sssaj1999.03615995006300030033x. 1999.

Meijide, A., Manca, G., Goded, I., Magliulo, V., Di Tommasi, P., Seufert, G., & Cescatti, A. Seasonal trends and environmental controls of methane emissions in a rice paddy field in Northern Italy. Biogeosciences, 8(12), 3809. https://doi.org/10.5194/bg-8-3809-2011. 2011.

Melloh, R. A., & Crill, P. M. Winter methane dynamics in a temperate peatland. Global Biogeochem. Cy., 10(2), 247–254. https://doi.org/10.1029/96gb00365. 1996.

Melton, J. R., Wania, R., Hodson, E. L., Poulter, B., Ringeval, B., Spahni, R., Bohn, T., Avis, C. A., Beerling, D. J., Chen, G., Eliseev, A. V., Denisov, S. N., Hopcroft, P. O., Lettenmaier, D. P., Riley, W. J., Singarayer, J. S., Subin, Z. M., Tian, H., Zürcher, S., & Others. Present state of global wetland extent and wetland methane modelling: conclusions from a model inter-comparison project (WETCHIMP). Biogeosciences, 10(2), 753–788. https://doi.org/10.5194/bg-10-753-2013. 2013.

Merbold, Lutz, Corinna Rebmann, & Chiara Corradi. FLUXNET-CH4 RU-Che Cherski. Russian Federation. https://doi:10.18140/FLX/1669655. 2020.

Meyer, H., & Pebesma, E. Predicting into unknown space? Estimating the area of applicability of spatial prediction models. arXiv [stat.ML]. arXiv. http://arxiv.org/abs/2005.07939. 2020.

Mishra, S. R., Pattnaik, P., Sethunathan, N., & Adhya, T. K. Anion-Mediated Salinity Affecting Methane Production in a Flooded Alluvial Soil. Geomicrobiol. J., 20(6), 579–586. https://doi.org/10.1080/713851167. 2003.

Moffat, A. M., Papale, D., Reichstein, M., Hollinger, D. Y., Richardson, A. D., Barr, A. G., Beckstein, C., Braswell, B. H., Churkina, G., Desai, A. R., Falge, E., Gove, J. H., Heimann, M., Hui, D., Jarvis, A. J., Kattge, J., Noormets, A., & Stauch, V. J. Comprehensive comparison of gap-filling techniques for eddy covariance net carbon fluxes. Agr. Forest Meteorol., 147(3), 209–232. https://doi.org/10.1016/j.agrformet.2007.08.011. 2007.

Myhre, G., D. Shindell, F.-M. Bréon, W. Collins, J. Fuglestvedt, J. Huang, D. Koch, J.-F. Lamarque, D. Lee, B. Mendoza, T. Nakajima, A. Robock, G. Stephens, T. Takemura and H. Zhang. Anthropogenic and Natural Radiative Forcing Supplementary Material. In Stocker, T.F., D. Qin, G.-K. Plattner, M. Tignor, S.K. Allen, J. Boschung, A. Nauels, Y. Xia, V. Bex and P.M. Midgley (Ed.), Climate Change 2013: The Physical Science Basis. Contribution of Working Group I to the Fifth Assessment Report of the Intergovernmental Panel on Climate Change. 2013.

Nemitz, E., Mammarella, I., Ibrom, A., Aurela, M., Burba, G. G., Dengel, S., Gielen, B., Grelle, A., Heinesch, B., Herbst, M., Hörtnagl, L., Klemedtsson, L., Lindroth, A., Lohila, A., McDermitt, D. K., Meier, P., Merbold, L., Nelson, D., Nicolini, G., & Others. Standardisation of eddy-covariance flux measurements of methane and nitrous oxide. Int. Agrophy., 32(4), 517–549. https://doi.org/10.1515/intag-2017-0042. 2018.

Nielsen, H. B. Damping parameter in Marquardt's method. Department of Mathematical Modeling, IMM, Technical University of Denmark. Technical Report, IMM-REP-1999-05. 1999.

Nilsson, Mats B., & Matthias Peichl. FLUXNET-CH4 SE-Deg Degero. Sweden. https://doi:10.18140/FLX/1669659. 2020.

Niu, Shuli, & Weinan Chen. FLUXNET-CH4 CN-Hgu Hongyuan. China. https://doi:10.18140/FLX/1669632. 2020.

Noormets, Asko, John King, Bhaskar Mitra, Guofang Miao, Maricar Aguilos, Kevan Minick, Prajaya Prajapati, Jean-Christophe Domec, Jonathan Furst, & Maxwell Wightman. FLUXNET-CH4 US-NC4 NC_AlligatorRiver. United States. https://doi:10.18140/FLX/1669686. 2020.

Oikawa, P. Y., Jenerette, G. D., Knox, S. H., Sturtevant, C., Verfaillie, J., Dronova, I., Poindexter, C. M., Eichelmann, E., & Baldocchi, D. D. Evaluation of a hierarchy of models reveals importance of substrate limitation for predicting carbon dioxide and methane exchange in restored wetlands. J. Geophys. Res.-Biogeo., 122(1), 145–167. https://doi.org/10.1002/2016JG003438. 2017.

Oikawa, Patty. FLUXNET-CH4 US-EDN Eden Landing Ecological Reserve. United States. https://doi:10.18140/FLX/1669673. 2020.

Olefeldt, D., Turetsky, M. R., Crill, P. M., & McGuire, A. D. Environmental and physical controls on northern terrestrial methane emissions across permafrost zones. Glob. Change Biol., 19(2), 589–603. https://doi.org/10.1111/gcb.12071. 2013.

Papale, D., Andrew Black, T., Carvalhais, N., Cescatti, A., Chen, J., Jung, M., Kiely, G., Lasslop, G., Mahecha, M. D., Margolis, H., Merbold, L., Montagnani, L., Moors, E., Olesen, J. E., Reichstein, M., Tramontana, G., van Gorsel, E., Wohlfahrt, G., & Ráduly, B. Effect of spatial sampling from European flux towers for estimating carbon and water fluxes with artificial neural networks. J. Geophys. Res.-Biogeo., 120(10), 1941–1957. https://doi.org/10.1002/2015jg002997. 2015.

Parmentier, F. J. W., van Huissteden, J., van der Molen, M. K., Schaepman-Strub, G., Karsanaev, S. A., Maximov, T. C., & Dolman, A. J. Spatial and temporal dynamics in eddy covariance observations of methane fluxes at a tundra site in northeastern Siberia. J. Geophys. Res., 116(G3), 1368. https://doi.org/10.1029/2010JG001637. 2011.

Pastorello, G., Trotta, C., Canfora, E., Chu, H., Christianson, D., Cheah, Y.-W., Poindexter, C., Chen, J., Elbashandy, A., Humphrey, M., Isaac, P., Polidori, D., Ribeca, A., van Ingen, C., Zhang, L., Amiro, B., Ammann, C., Arain, M. A., Ardö, J., & Others. The FLUXNET2015 dataset and the ONEFlux processing pipeline for eddy covariance data. Scientific Data, 7(1), 225. https://doi.org/10.1038/s41597-020-0534-3. 2020.

Pattnaik, P., Mishra, S. R., Bharati, K., Mohanty, S. R., Sethunathan, N., & Adhya, T. K. Influence of salinity on methanogenesis and associated microflora in tropical rice soils. Microbiol. Res., 155(3), 215–220. https://doi.org/10.1016/S0944-5013(00)80035-X. 2000.

Poffenbarger, H. J., Needelman, B. A., & Patrick Megonigal, J. Salinity Influence on Methane Emissions from Tidal Marshes. Wetlands, 31(5), 831–842. https://doi.org/10.1007/s13157-011-0197-0. 2011.

Poulter, B., Bousquet, P., Canadell, J. G., Ciais, P., Peregon, A., Saunois, M., Arora, V. K., Beerling, D. J., Brovkin, V., Jones, C. D., Joos, F., Gedney, N., Ito, A., Kleinen, T., Koven, C. D., McDonald, K., Melton, J. R., Peng, C., Peng, S., & Others. Global wetland contribution to 2000–2012 atmospheric methane growth rate dynamics. Environ. Res. Lett., 12(9), 094013. https://doi.org/10.1088/1748-9326/aa8391. 2017.

Reba, Michele, Benjamin Runkle, & Kosana Suvocarev. FLUXNET-CH4 US-HRC Humnoke Farm Rice Field – Field C. United States. https://doi:10.18140/FLX/1669677. 2020.

Reichstein, M., Falge, E., Baldocchi, D., Papale, D., Aubinet, M., Berbigier, P., Bernhofer, C., Buchmann, N., Gilmanov, T., Granier, A., Grunwald, T., Havrankova, K., Ilvesniemi, H., Janous, D., Knohl, A., Laurila, T., Lohila, A., Loustau, D., Matteucci, G., & Others. On the separation of net ecosystem exchange into assimilation and ecosystem respiration: review and improved algorithm. Glob. Change Biol., 11(9), 1424–1439). https://doi.org/10.1111/j.1365-2486.2005.001002.x. 2005.

Rey-Sanchez, Camilo, Daphne Szutu, Robert Shortt, Samuel D. Chamberlain, Joseph Verfaillie, & Dennis Baldocchi. FLUXNET-CH4 US-Bi1 Bouldin Island Alfalfa. United States. https://doi:10.18140/FLX/1669666. 2020a.

Rey-Sanchez, Camilo, Daphne Szutu, Kyle Hemes, Joseph Verfaillie, & Dennis Baldocchi. FLUXNET-CH4 US-Bi2 Bouldin Island corn. United States. https://doi:10.18140/FLX/1669667. 2020b.

Richardson, A. D., Hollinger, D. Y., Burba, G. G., Davis, K. J., Flanagan, L. B., Katul, G. G., William Munger, J., Ricciuto, D. M., Stoy, P. C., Suyker, A. E., Verma, S. B., & Wofsy, S. C. A multi-site analysis of random error in tower-based measurements of carbon and energy fluxes. Agr. Forest Meteorol., 136(1), 1–18. https://doi.org/10.1016/j.agrformet.2006.01.007. 2006.

Richardson, A. D., & Hollinger, D. Y. A method to estimate the additional uncertainty in gap-filled NEE resulting from long gaps in the CO2 flux record. Agr. Forest Meteorol., 147(3), 199–208. https://doi.org/10.1016/j.agrformet.2007.06.004. 2007.

Richardson, A. D., Mahecha, M. D., Falge, E., Kattge, J., Moffat, A. M., Papale, D., Reichstein, M., Stauch, V. J., Braswell, B. H., Churkina, G., Kruijt, B., & Hollinger, D. Y. Statistical properties of random CO2 flux measurement uncertainty inferred from model residuals. Agr. Forest Meteorol., 148(1), 38–50. https://doi.org/10.1016/j.agrformet.2007.09.001. 2008.

Richardson, A. D., Aubinet, M., Barr, A. G., Hollinger, D. Y., Ibrom, A., Lasslop, G., & Reichstein, M. Uncertainty quantification. Eddy Covariance: A Practical Guide to Measurement and Data Analysis. (eds) Aubinet, M., Vesala, T., Papale, D. Springer Atmospheric Sciences. 2012.

Richardson, Andrew D, & David Y Hollinger. FLUXNET-CH4 US-Ho1 Howland Forest (main tower). United States. https://doi:10.18140/FLX/1669675. 2020.

Rinne, J., Riutta, T., Pihlatie, M., Aurela, M., Haapanala, S., Tuovinen, J.-P., Tuittila, E.-S., & Vesala, T. Annual cycle of methane emission from a boreal fen measured by the eddy covariance technique. Tellus B, 59(3), 449–457. https://doi.org/10.1111/j.1600-0889.2007.00261.x. 2007.

Runkle, B. R. K., Suvočarev, K., Reba, M. L., Reavis, C. W., Smith, S. F., Chiu, Y.-L., & Fong, B. Methane Emission Reductions from the Alternate Wetting and Drying of Rice Fields Detected Using the Eddy Covariance Method. Envir. Sci. Tech., 53(2), 671–681. https://doi.org/10.1021/acs.est.8b05535. 2019.
Runkle, Benjamin, Michele Reba, & Kosana Suvocarev. FLUXNET-CH4 US-HRA Humnoke Farm Rice Field – Field A. United States. https://doi:10.18140/FLX/1669676. 2020.
Ryu, Youngryel, Minseok Kang, & Jongho Kim. FLUXNET-CH4 KR-CRK Cheorwon Rice paddy. Korea, Republic of. https://doi:10.18140/FLX/1669649. 2020.
Sachs, T., Giebels, M., Boike, J., & Kutzbach, L. Environmental controls on CH4 emission from polygonal tundra on the microsite scale in the Lena river delta, Siberia: CONTROLS ON TUNDRA CH4 FLUX AND SCALING. Glob. Change Biol., 16(11) 3096 – 3110. https://doi.org/10.1111/j.1365-2486.2010.02232.x. 2010.
Sachs, Torsten, Christian Wille, & Eric Larmanou. FLUXNET-CH4 DE-Dgw Dagowsee. Germany. https://doi:10.18140/FLX/1669633. 2020a.
Sachs, Torsten, Christian Wille, Eric Larmanou, & Daniela Franz. FLUXNET-CH4 DE-Zrk Zarnekow. Germany. https://doi:10.18140/FLX/1669636. 2020b.
Sakabe, Ayaka, Masayuki Itoh, Takashi Hirano, & Kitso Kusin. FLUXNET-CH4 ID-Pag Palangkaraya undrained forest. Indonesia. https://doi:10.18140/FLX/1669643. 2020.
Saunois, M., Bousquet, P., Poulter, B., Peregon, A., Ciais, P., Canadell, J. G., Dlugokencky, E. J., Etiope, G., Bastviken, D., Houweling, S., Janssens-Maenhout, G., Tubiello, F. N., Castaldi, S., Jackson, R. B., Alexe, M., Arora, V. K., Beerling, D. J., Bergamaschi, P., Blake, D. R., & Others. The global methane budget 2000–2012. Earth Syst. Sci. Data, 8, 697-751. https://doi.org/10.5194/essd-8-697-2016. 2016.
Saunois, M., Stavert, A. R., Poulter, B., Bousquet, P., Canadell, J. G., Jackson, R. B., Raymond, P. A., Dlugokencky, E. J., Houweling, S., Patra, P. K., Ciais, P., Arora, V. K., Bastviken, D., Bergamaschi, P., Blake, D. R., Brailsford, G., Bruhwiler, L., Carlson, K. M., Carrol, M., & Others. The Global Methane Budget 2000–2017. Earth Syst. Sci. Data, 12, 1561-1623. https://doi.org/10.5194/essd-12-1561-2020. 2020.
Schafer, Karina. FLUXNET-CH4 US-MRM Marsh Resource Meadowlands Mitigation Bank. United States. https://doi:10.18140/FLX/1669684. 2020.
Schuur, E.A. FLUXNET-CH4 US-EML Eight Mile Lake Permafrost thaw gradient, Healy Alaska. United States. https://doi:10.18140/FLX/1669674. 2020.
Seyfferth, A. L., Bothfeld, F., Vargas, R., Stuckey, J. W., Wang, J., Kearns, K., Michael, H. A., Guimond, J., Yu, X., & Sparks, D. L. Spatial and temporal heterogeneity of geochemical controls on carbon cycling in a tidal salt marsh. Geochim. Cosmochim. Ac., 282, 1–18. https://doi.org/10.1016/j.gca.2020.05.013. 2020.
Shortt, Robert, Kyle Hemes, Daphne Szutu, Joseph Verfaillie, & Dennis Baldocchi. FLUXNET-CH4 US-Sne Sherman Island Restored Wetland. United States. https://doi:10.18140/FLX/1669693. 2020.
Sims, D. A., Rahman, A. F., Cordova, V. D., El-Masri, B. Z., Baldocchi, D. D., Flanagan, L. B., Goldstein, A. H., Hollinger, D. Y., Misson, L., Monson, R. K., Oechel, W. C., Schmid, H. P., Wofsy, S. C., & Xu, L. On the use of MODIS EVI to assess gross primary productivity of North American ecosystems. J. Geophys. Res.-Biogeo. 111(G4). https://doi.org/10.1029/2006jg000162. 2006.
Sonnentag, Oliver, & Manuel Helbig. FLUXNET-CH4 CA-SCB Scotty Creek Bog. Canada. https://doi:10.18140/FLX/1669613. 2020a.
Sonnentag, Oliver, & Manuel Helbig. FLUXNET-CH4 CA-SCC Scotty Creek Landscape. Canada. https://doi:10.18140/FLX/1669628. 2020b.
Spahni, R., Wania, R., Neef, L., van Weele, M., Pison, I., Bousquet, P., Frankenberg, C., Foster, P. N., Joos, F., Prentice, I. C., & van Velthoven, P. Constraining global methane emissions and uptake by ecosystems. In Biogeosciences, 8(6), 1643–1665. https://doi.org/10.5194/bg-8-1643-2011. 2011.
Sparks, Jed P. FLUXNET-CH4 US-MAC MacArthur Agro-Ecology. United States. https://doi:10.18140/FLX/1669683. 2020.
Sturtevant, C. S., Ruddell, B. L., Knox, S. H., Verfaillie, J. G., Matthes, J. H., Oikawa, P. Y., & Baldocchi, D. D. Identifying scale-emergent, nonlinear, asynchronous processes of wetland methane exchange. J. Geophys. Res.-Biogeo., 121, 188–204. https://doi.org/10.1002/2015JG003054. 2016.
Tagesson, T., Mölder, M., Mastepanov, M., Sigsgaard, C., Tamstorf, M. P., Lund, M., Falk, J. M., Lindroth, A., Christensen, T. R., & Ström, L. Land-atmosphere exchange of methane from soil thawing to soil freezing in a high-Arctic wet tundra ecosystem. Glob. Change Biol., 18(6), 1928–1940. https://doi.org/10.1111/j.1365-2486.2012.02647.x. 2012.

~~Tang, Angela Che Ing,~~ Guan Xhuan Wong, Lulie Melling, Angela Che Ing Tang, Edward Baran Aeries, Joseph Wenceslaus Waili, Kevin Kemudang Musin, Kim San Lo, & Frankie Kiew. FLUXNET-CH4 MY-MLM Maludam National Park. Malaysia. https://doi:10.18140/FLX/1669650. 2020.

Taoka, T., Iwata, H., Hirata, R., Takahashi, Y., Miyabara, Y., & Itoh, M. Environmental Controls on Diffusive and Ebullitive Methane Emission at a Sub-Daily Time Scale in the Littoral Zone of a Mid-Latitude Shallow Lake. J. Geophys. Res.-Biogeo., 125(9), https://doi.org/10.1029/2020JG005753. 2020.

Torn, Margaret, & Sigrid Dengel. FLUXNET-CH4 US-NGB NGEE Arctic Barrow. United States. https://doi:10.18140/FLX/1669687. 2020a.

Torn, Margaret, & Sigrid Dengel. FLUXNET-CH4 US-NGC NGEE Arctic Council. United States. https://doi:10.18140/FLX/1669688. 2020b.

Treat, C. C., Anthony Bloom, A., & Marushchak, M. E. Nongrowing season methane emissions-a significant component of annual emissions across northern ecosystems. Glob. Change Biol., 24(8), 3331–3343. https://doi.org/10.1111/gcb.14137. 2018.

Turetsky, M. R., Kotowska, A., Bubier, J., Dise, N. B., Crill, P., Hornibrook, E. R. C., Minkkinen, K., Moore, T. R., Myers-Smith, I. H., Nykänen, H., Olefeldt, D., Rinne, J., Saarnio, S., Shurpali, N., Tuittila, E.-S., Waddington, J. M., White, J. R., Wickland, K. P., & Wilmking, M. A synthesis of methane emissions from 71 northern, temperate, and subtropical wetlands. Glob. Change Biol., 20(7), 2183–2197. https://doi.org/10.1111/gcb.12580. 2014.

Ueyama, Masahito, Takashi Hirano, & Yasuhiro Kominami. FLUXNET-CH4 JP-BBY Bibai bog. Japan. https://doi:10.18140/FLX/1669646. 2020.

Valach, Alex, Daphne Szutu, Elke Eichelmann, Sara Knox, Joseph Verfaillie, & Dennis Baldocchi. FLUXNET-CH4 US-Tw1 Twitchell Wetland West Pond. United States. https://doi:10.18140/FLX/1669696. 2020a.

Valach, Alex, Kuno Kasak, Daphne Szutu, Joseph Verfaillie, & Dennis Baldocchi. FLUXNET-CH4 US-Tw5 East Pond Wetland. United States. https://doi:10.18140/FLX/1669699. 2020b.

Varlagin, Andrej. FLUXNET-CH4 RU-Fy2 Fyodorovskoye dry spruce. Russian Federation. https://doi:10.18140/FLX/1669657. 2020.

Vazquez-Lule, Alma, & Rodrigo Vargas. FLUXNET-CH4 US-StJ St Jones Reserve. United States. https://doi:10.18140/FLX/1669695. 2020.

Vázquez-Lule, A., & Vargas, R. Biophysical drivers of net ecosystem and methane exchange across phenological phases in a tidal salt marsh. Agricultural and Forest Meteorology, 300, 108309. https://doi.org/10.1016/j.agrformet.2020.108309. 2021.

Verma, S. B., Ullman, F. G., Billesbach, D., Clement, R. J., Kim, J., & Verry, E. S. Eddy correlation measurements of methane flux in a northern peatland ecosystem. Bound. Lay. Meteorol., 58(3), 289–304. https://doi.org/10.1007/BF02033829. 1992.

Vesala, Timo, Eeva-Stiina Tuittila, Ivan Mammarella, & Pavel Alekseychik. FLUXNET-CH4 FI-Si2 Siikaneva-2 Bog. Finland. https://doi:10.18140/FLX/1669639. 2020a.

Vesala, Timo, Eeva-Stiina Tuittila, Ivan Mammarella, & Janne Rinne. FLUXNET-CH4 FI-Sii Siikaneva. Finland. https://doi:10.18140/FLX/1669640. 2020b.

Villarreal, S., Guevara, M., Alcaraz-Segura, D., Brunsell, N. A., Hayes, D., Loescher, H. W., & Vargas, R. Ecosystem functional diversity and the representativeness of environmental networks across the conterminous United States. Agr. Forest Meteorol., 262, 423–433. https://doi.org/10.1016/j.agrformet.2018.07.016. 2018.

Villarreal, S., Guevara, M., Alcaraz-Segura, D., & Vargas, R. Optimizing an Environmental Observatory Network Design Using Publicly Available Data. J. Geophys. Res.-Biogeo., 124(7), 1812–1826. https://doi.org/10.1029/2018JG004714. 2019.

Vourlitis, George, Higo Dalmagro, Jose de S. Nogueira, Mark Johnson, & Paulo Arruda. FLUXNET-CH4 BR-Npw Northern Pantanal Wetland. Brazil. https://doi:10.18140/FLX/1669368. 2020.

Vuichard, N., & Papale, D. Filling the gaps in meteorological continuous data measured at FLUXNET sites with ERA-Interim reanalysis. Earth Syst. Sci. Data, 7(2), 157–171. https://doi.org/10.5194/essd-7-157-2015. 2015.

Weston, N. B., Dixon, R. E., & Joye, S. B. Ramifications of increased salinity in tidal freshwater sediments: Geochemistry and microbial pathways of organic matter mineralization. J. Geophys. Res., 111(G1). https://doi.org/10.1029/2005jg000071. 2006.

Weston, N. B., Vile, M. A., Neubauer, S. C., & Velinsky, D. J. Accelerated microbial organic matter mineralization following salt-water intrusion into tidal freshwater marsh soils. Biogeochemistry, 102, 135–151. https://doi.org/10.1007/s10533-010-9427-4. 2011.

Wik, M., Crill, P. M., Varner, R. K., & Bastviken, D. Multiyear measurements of ebullitive methane flux from three subarctic lakes. J. Geophys. Res.-Biogeo. 118(3), 1307–1321. https://doi.org/10.1002/jgrg.20103. 2013.

Windham-Myers, Lisamarie, Ellen Stuart-Haëntjens, Brian Bergamaschi, Sara Knox, Frank Anderson, & Kyle Nakatsuka. FLUXNET-CH4 US-Srr Suisun marsh - Rush Ranch. United States. https://doi:10.18140/FLX/1669694. 2020.

Wohlfahrt, Georg, Albin Hammerle, & Lukas Hörtnagl. FLUXNET-CH4 AT-Neu Neustift. Austria. https://doi:10.18140/FLX/1669365. 2020.

Wutzler, T., Lucas-Moffat, A., Migliavacca, M., Knauer, J., Sickel, K., Šigut, L., Menzer, O., & Reichstein, M. Basic and extensible post-processing of eddy covariance flux data with REddyProc. Biogeosciences, 15, 5015–5030. https://doi.org/10.5194/bg-2018-56-sc1. 2018.

Xu, X., Riley, W. J., Koven, C. D., Billesbach, D. P., -W. Chang, R. Y., Commane, R., Euskirchen, E. S., Hartery, S., Harazono, Y., Iwata, H., McDonald, K. C., Miller, C. E., Oechel, W. C., Poulter, B., Raz-Yaseef, N., Sweeney, C., Torn, M., Wofsy, S. C., Zhang, Z., & Zona, D. A multi-scale comparison of modeled and observed seasonal methane emissions in northern wetlands. Biogeosciences, 13(17), 5043–5056. https://doi.org/10.5194/bg-13-5043-2016. 2016.

Yvon-Durocher, G., Allen, A. P., Bastviken, D., Conrad, R., Gudasz, C., St-Pierre, A., Thanh-Duc, N., & del Giorgio, P. A. Methane fluxes show consistent temperature dependence across microbial to ecosystem scales. Nature, 507(7493), 488–491. https://doi.org/10.1038/nature13164. 2014.

Zhang, Z. Fluet-Choinard, E., Jensen, K, McDonald, K, Hugelius, G, Gumbricht, T., Carrol, M., Prigent, C., Bartsch, A., & Poulter, B. Development of a global dataset of Wetland Area and Dynamics for Methane Modeling (WAD2M) [Data set]. Zenodo. http://doi.org/10.5281/zenodo.3998454. 2020.

Zhang, Z. Fluet-Choinard, E., Jensen, K, McDonald, K, Hugelius, G, Gumbricht, T., Carrol, M., Prigent, C., Bartsch, A., & Poulter, B. Development of a global dataset of Wetland Area and Dynamics for Methane Modeling (WAD2M). Earth Syst. Sci. Data [In press]. 2021.

Zona, D., Gioli, B., Commane, R., Lindaas, J., Wofsy, S. C., Miller, C. E., Dinardo, S. J., Dengel, S., Sweeney, C., Karion, A., Chang, R. Y.-W., Henderson, J. M., Murphy, P. C., Goodrich, J. P., Moreaux, V., Liljedahl, A., Watts, J. D., Kimball, J. S., Lipson, D. A., & Oechel, W. C. Cold season emissions dominate the Arctic tundra methane budget. P. Natl. A. Sci. USA., 113(1), 40–45. https://doi.org/10.1073/pnas.1516017113. 2016.

Zona, Donatella, & Walter C Oechel. FLUXNET-CH4 US-Atq Atqasuk. United States. https://doi:10.18140/FLX/1669663. 2020a.

Zona, Donatella, & Walter C Oechel. FLUXNET-CH4 US-Beo Barrow Environmental Observatory (BEO) tower. United States. https://doi:10.18140/FLX/1669664. 2020b.

Zona, Donatella, & Walter C Oechel. FLUXNET-CH4 US-Bes Barrow-Bes (Biocomplexity Experiment South tower). United States. https://doi:10.18140/FLX/1669665. 2020c.

Zona, Donatella, & Walter C Oechel. FLUXNET-CH4 US-Ivo Ivotuk. United States. https://doi:10.18140/FLX/1669679. 2020d.

APPENDIX A

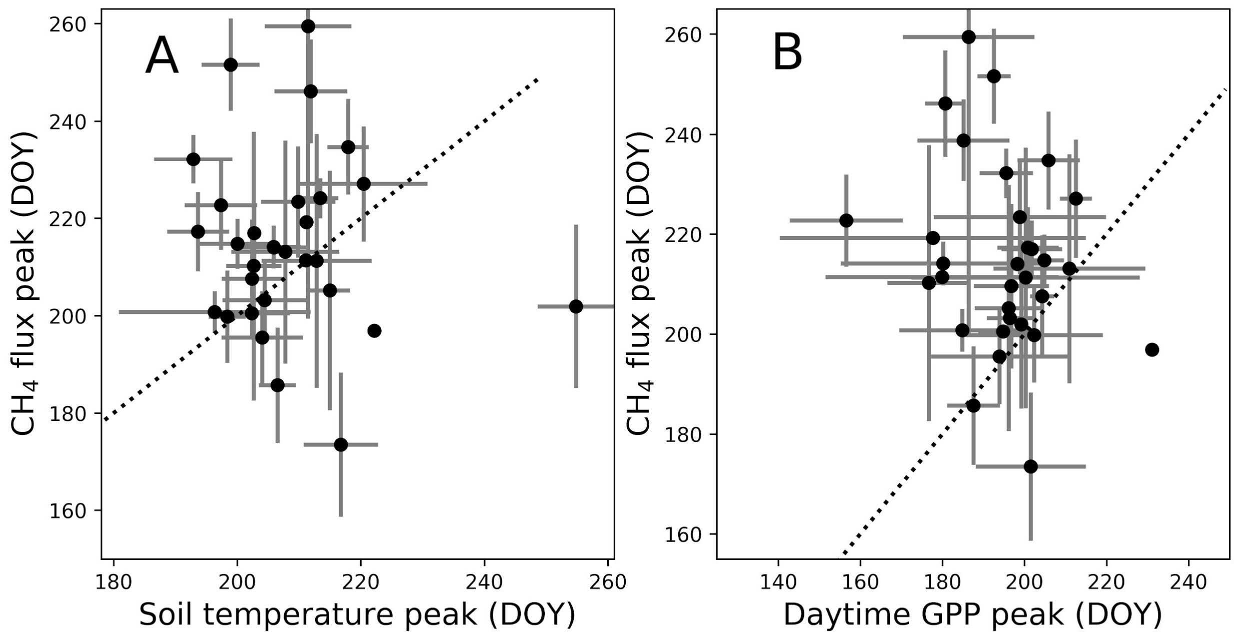

Figure A1: Peak methane (CH_4) flux timing versus peak gross primary productivity (GPP) timing (A) and peak soil temperature timing by day of year (B). Points represent site average and error bars represent standard deviations. Dotted line represents 1:1 relationship.

APPENDIX B

Table B1: Data variable names, descriptions, and units

FLUXNET-CH4 Data Variables

This webpage describes data variables and file formatting for the FLUXNET-CH4 Community Product.

1. Data Variable: Base names

Base names indicate fundamental quantities that are either measured or calculated/derived. They can also indicate quantified quality information.

Table 1. Base names for data variables

Variable	***Description***	***Units***
TIMEKEEPING		
TIMESTAMP_START	ISO timestamp start of averaging period, used in half-hourly data	YYYYMMDDHHMM
TIMESTAMP_END	ISO timestamp end of averaging period, used in half-hourly data	YYYYMMDDHHMM
TIMESTAMP	ISO timestamp used in daily aggregation files	YYYYMMDD
MET_RAD		
SW_IN	Shortwave radiation, incoming	W m-2
SW_OUT	Shortwave radiation, outgoing	W m-2
LW_IN	Longwave radiation, incoming	W m-2
LW_OUT	Longwave radiation, outgoing	W m-2

PPFD_IN	Photosynthetic photon flux density, incoming	µmolPhoton m-2 s-1
PPFD_OUT	Photosynthetic photon flux density, outgoing	µmolPhoton m-2 s-1
NETRAD	Net radiation	W m-2

MET_WIND

USTAR	Friction velocity	m s-1
WD	Wind direction	Decimal degrees
WS	Wind speed	m s-1

HEAT

H	Sensible heat turbulent flux (with storage term if provided by site PI)	W m-2
LE	Latent heat turbulent flux (with storage term if provided by site PI)	W m-2
G	Soil heat flux	W m-2

MET_ATM

PA	Atmospheric pressure	kPa
TA	Air temperature	deg C

VPD	Vapor Pressure Deficit	hPa
RH	Relative humidity, range 0-100	%
MET_PRECIP		
P	Precipitation	mm
PRODUCTS		
NEE	Net Ecosystem Exchange	µmolCO2 m-2 s-1
GPP	Gross primary productivity	µmolCO2 m-2 s-1
RECO	Ecosystem respiration	µmolCO2 m-2 s-1
GASES		
FCH4	Methane (CH4) turbulent flux (no storage correction)	nmolCH4 m-2 s-1
MET_SOIL		
TS	Soil temperature	deg C
WTD	Water table depth (negative values indicate below the surface)	m

2. Data Variable: Qualifiers

Qualifiers are suffixes appended to variable base names that provide additional information about the variable. For example, the _DT qualifier in the variable label GPP_DT indicates that gross primary production (GPP) has been partitioned using the flux partitioning method from Lasslop et al. 2010.

Multiple qualifiers can be added, and they must **follow the order in which they are presented here**.

2.1. Qualifiers: General

General qualifiers indicate additional information about a variable.

- **_F :** Variable has been gap-filled by the FLUXNET-CH4 team. Gaps in meteorological variables (including air temperature (TA), incoming shortwave (SW_IN) and longwave (LW_IN) radiation, vapor pressure deficit (VPD), pressure (PA), precipitation (P), and wind speed (WS)) were filled with ERA-Interim (ERA-I) reanalysis data ((Vuichard and Papale 2015)). Other variables were filled using the MDS approach in REddyProc (see Delwiche et al. 2020 for more details).

- **_DT :** Variable acquired using the flux partitioning method from (Lasslop et al. 2010), with values estimated by fitting the light-response curve.

- **_NT :** Variable acquired using the flux partitioning method from (Reichstein et al. 2005), with values estimated from night-time data and extrapolated to day time.

- **_RANDUNC:** Random uncertainty introduced from several different sources including errors associated with the flux measurement system (gas analyzer, sonic anemometer, data acquisition system, flux calculations), errors associated with turbulent transport, and statistical errors relating to the location and activity of the sites of flux exchange ("footprint heterogeneity") (Hollinger and Richardson 2005).

- **_ANNOPTLM :** Gap-filled variable using an artificial neural net routine from Matlab with the Levenberg-Marquardt algorithm as the training function, and parameters optimized across runs (more detail in (Sara Helen Knox et al. 2016; Sara H. Knox et al. 2019)).

- **_UNC :** Uncertainty introduced from ANNOPTLM gap-filling routine, as described in Knox et al. 2016 and Knox et al. 2019.

- **_QC :** Reports quality checks on FCH4 gap-filled data (_ANNOPTLM) based on length of data gap. 1 = data gap shorter than 2 months, 3 = data gap exceeds 2 months which could lead to poor quality gap-filled data. Nondimensional.

2.2. Qualifiers: Positional *(_V)*

Positional qualifiers are used to indicate relative positions of observations at the site. For FLUXNET-CH4, positional qualifiers are used to distinguish soil temperature probes for sites with more than one probe. Probe depths for each positional qualifier per site are included in the metadata file included with data download and also in Table B7 of Delwiche et al. 2020. For sites where the original database file release in Ameriflux, AsiaFlux, or EuroFlux contains multiple probes at the same _V depth, we average values and report only the average for each _V position. The one exception to this is site US-UAF where the original positional qualifier from the data we downloaded from Ameriflux had different depths for the same qualifier. We still averaged the probe data, so _V qualifiers from US-UAF represent an average of more than one depth.

3.0 Missing data

Missing data are reported using -9999. Data for all days in a leap year are reported.

4.0 References

Hollinger, D. Y., and A. D. Richardson. 2005. “Uncertainty in Eddy Covariance Measurements and Its Application to Physiological Models.” *Tree Physiology* 25 (7): 873–85.

Knox, Sara Helen, Jaclyn Hatala Matthes, Cove Sturtevant, Patricia Y. Oikawa, Joseph Verfaillie, and Dennis Baldocchi. 2016. “Biophysical Controls on Interannual Variability in Ecosystem-Scale CO2and CH4exchange in a California Rice Paddy.” *Journal of Geophysical Research: Biogeosciences*. https://doi.org/10.1002/2015jg003247.

Knox, Sara H., Robert B. Jackson, Benjamin Poulter, Gavin McNicol, Etienne Fluet-Chouinard, Zhen Zhang, Gustaf Hugelius, et al. 2019. “FLUXNET-CH4 Synthesis Activity: Objectives, Observations, and Future Directions.” *Bulletin of the American Meteorological Society* 100 (12): 2607–32.

Lasslop, Gitta, Markus Reichstein, Dario Papale, Andrew D. Richardson, Almut Arneth, Alan Barr, Paul Stoy, and Georg Wohlfahrt. 2010. “Separation of Net Ecosystem Exchange into Assimilation and Respiration Using a Light Response Curve Approach: Critical Issues and Global Evaluation.” *Global Change Biology*. https://doi.org/10.1111/j.1365-2486.2009.02041.x.

Reichstein, Markus, Eva Falge, Dennis Baldocchi, Dario Papale, Marc Aubinet, Paul Berbigier, Christian Bernhofer, et al. 2005. “On the Separation of Net Ecosystem Exchange into Assimilation and Ecosystem Respiration: Review and Improved Algorithm.” *Global Change Biology*. https://doi.org/10.1111/j.1365-2486.2005.001002.x.

Vuichard, N., and D. Papale. 2015. “Filling the Gaps in Meteorological Continuous Data Measured at FLUXNET Sites with ERA-Interim Reanalysis.” *Earth System Science Data*. https://doi.org/10.5194/essd-7-157-2015.